UNIVERSIDADE FEDERAL DE SANTA CATARINA
CENTRO TECNOLÓGICO
CURSO DE GRADUAÇÃO EM ENGENHARIA MECÂNICA

Pedro Alonso Condessa

DEVELOPMENT OF DYNAMIC MODEL OF PRESSURIZED HYDRAULIC RESERVOIR FOR APPLICATION IN AIRCRAFT

FLORIANÓPOLIS
2024

Pedro Alonso Condessa

DEVELOPMENT OF DYNAMIC MODEL OF PRESSURIZED HYDRAULIC RESERVOIR FOR APPLICATION IN AIRCRAFT

Trabalho de Conclusão do Curso submetido ao curso de Engenharia Mecânica do Centro Tecnológico da Universidade Federal de Santa Catarina como requisito parcial para a obtenção do título de Bacharel em Engenharia Mecânica.

Orientador: Prof. Marcos Paulo Nostrani, Dr. Eng.
Coorientador: Prof. Victor Juliano De Negri, Dr. Eng.

FLORIANÓPOLIS
2024

Condessa, Pedro Alonso
DEVELOPMENT OF DYNAMIC MODEL OF PRESSURIZED HYDRAULIC RESERVOIR FOR APPLICATION IN AIRCRAFT / Pedro Alonso Condessa ; orientador, Marcos Paulo Nostrani, coorientador, Victor Juliano De Negri, 2024.
84 p.

Trabalho de Conclusão de Curso (graduação) - Universidade Federal de Santa Catarina, Centro Tecnológico, Graduação em Engenharia Mecânica, Florianópolis, 2024.

Inclui referências.

1. Engenharia Mecânica. 2. Engenharia Mecânica. 3. Controle de Posição. 4. Sistemas Hidráulicos. I. Nostrani, Marcos Paulo. II. De Negri, Victor Juliano. III. Universidade Federal de Santa Catarina. Graduação em Engenharia Mecânica. IV. Título.

Pedro Alonso Condessa

DEVELOPMENT OF DYNAMIC MODEL OF PRESSURIZED HYDRAULIC RESERVOIR FOR APPLICATION IN AIRCRAFT.

Este Trabalho de Conclusão de Curso foi julgado adequado para obtenção do título de Engenheiro Mecânico e aprovado em sua forma final pelo Curso de Engenharia Mecânica.

Florianópolis, 20 de dezembro de 2024.

Documento assinado digitalmente
Carlos Enrique Nino Bohorquez
Data: 18/05/2026 16:36:43-0300
CPF: ***.878.519-**
Verifique as assinaturas em https://v.ufsc.br

Prof. Carlos Enrique Niño Bohórquez, Dr. Eng.

Coordenador do Curso

Banca Examinadora

Documento assinado digitalmente
Marcos Paulo Nostrani
Data: 18/05/2026 15:40:54-0300
CPF: ***.797.779-**
Verifique as assinaturas em https://v.ufsc.br

Prof. Marcos Paulo Nostrani, Dr.Eng

Orientador

Prof. Jonny Carlos da Silva, Dr.Eng

Universidade Federal de Santa Catarina

Documento assinado digitalmente
Antonio Carlos Valdiero
Data: 18/05/2026 16:05:17-0300
CPF: ***.227.377-**
Verifique as assinaturas em https://v.ufsc.br

Prof. Antônio Carlos Valdiero, Dr. Eng.

Universidade Federal de Santa Catarina

Florianópolis, 2024.

À minha família que,

amando-me, se priva da minha companhia

para que eu alcance minhas próprias conquistas.

AGRADECIMENTOS

Primeiramente, gostaria de agradecer aos meus pais, Ahikel e Fátima, por todo o apoio e amor que me deram ao longo da vida. Agradeço por tudo o que proporcionaram e pela dedicação constante, incentivando-me a nunca desistir, especialmente durante a realização deste trabalho de conclusão de curso. Sou eternamente grato por tudo que fizeram por mim, pois sou a pessoa que sou hoje graças a eles.

À minha irmã Alice, por toda amizade e companheirismo que sempre demonstrou.

Aos professores Marcos Paulo Nostrani e Victor Juliano De Negri, pela dedicação e apoio contínuos durante o desenvolvimento deste trabalho, sempre colaborando com dicas e sugestões, e mostrando se prontamente dispostos a ajudar sempre que possível, mesmo que estivessem com suas próprias responsabilidades a cumprir. Também por toda amizade no ano que estive trabalhando em seu laboratório – LASHIP, no qual pude aprimorar minhas capacidades técnicas como habilidades de comunicação.

Aos meus amigos Henrique Frassetto Cardoso, Arthur Vinícius Spiandorello Reitz, Lucas Massoni Pires, Bruno Vasel e João Victor Brochier Gonçalves, por sempre me proporcionarem bons momentos de convivência na faculdade, sempre estarem dispostos a ouvir meus desafios, por partilhar das alegrias de meus sucessos e por partilharem seus sucessos comigo, como se fossem os meus. Que a vida ilumine a vida profissional de vocês e que nunca se esqueçam de serem felizes. Viva os MC.

Aos meus colegas da Bosch, Paulo Leonel Teixeira, Cristiano Alexandre Boddenberg, Gabriel Linhares Baldo, Clovis Jandt, Lucio Batista Soares, Takaracy Haruyuki, Bruno Souza, Rodrigo Souto e Thiago Tomelin, por, mesmo com suas responsabilidades, dedicarem tempo para me ensinar sobre hidráulica e, mais importante ainda, sobre a vida.

Aos amigos do LASHIP, Túlio, Ruham Victor, Vanderlei, Flávio Filho, Nicollas Squillante, e tantos outros, pelo apoio, amizade e pelos conselhos durante o trabalho de conclusão de curso. Foi um prazer aprender e conviver com todos.

Por fim, agradeço ao curso de Engenharia Mecânica da Universidade Federal de Santa Catarina e aos seus professores, que me proporcionaram uma sólida formação técnica e, acima de tudo, me ensinaram a habilidade essencial para um engenheiro: a capacidade de aprender a aprender.

RESUMO

À medida que as aeronaves se tornaram maiores e mais complexas, a demanda por sistemas hidráulicos mais robustos e eficientes se tornou crítica. Para atender a essas demandas, foram desenvolvidos reservatórios pressurizados, como os de ar pressurizado, gás pressurizado e *bootstrap*, cada um garantindo pressão de sucção suficiente na entrada da bomba e desempenho estável sob condições operacionais variáveis. Este trabalho foca no reservatório *bootstrap*. O estudo investiga o projeto e a simulação de um sistema hidráulico pressurizado incorporando um reservatório *bootstrap* para aplicações aeronáuticas, abordando a estabilidade da pressão e o controle de posição de uma superfície de controle de voo em condições dinâmicas. Foi desenvolvido um modelo matemático para os componentes, incluindo o atuador, servo-válvula e reservatório *bootstrap*, para simular o comportamento do sistema. A metodologia proposta por Furst & De Negri (2002) foi aplicada para dimensionar os componentes hidráulicos, como o atuador e a servo-válvula, garantindo que o sistema atendesse aos requisitos de resposta dinâmica e controle de posição. Esses requisitos, como deslocamento máximo, tempo de acomodação e força de carga, foram confirmados nos resultados da simulação. O sistema alcançou pressão estável no reservatório e controle preciso de posição, com um tempo de acomodação de 0,975 segundos, atendendo à especificação de projeto de 1 segundo. Os resultados alinharam-se com o comportamento esperado do reservatório *bootstrap*, confirmando sua eficácia em manter a estabilidade do sistema e garantir o controle de posição sob condições dinâmicas. Esses resultados fornecem uma base para validação experimental futura e a possível integração do reservatório *bootstrap* em sistemas hidráulicos mais complexos.

Palavras-chave: Sistemas hidráulicos. Reservatório *bootstrap*. Reservatórios pressurizados. Simulação de sistemas hidráulicos.

RESUMO EXPANDIDO

Introdução

Com o aumento do tamanho e complexidade das aeronaves, houve uma crescente demanda por sistemas hidráulicos mais robustos e eficientes para atender às exigências operacionais. Os reservatórios hidráulicos pressurizados desempenham um papel crucial nesses sistemas, garantindo o fornecimento constante de fluido aos componentes e prevenindo a cavitação na entrada da bomba. Dentre as configurações mais utilizadas, destacam-se os reservatórios pressurizados a ar, gás e o tipo *bootstrap*, cada um apresentando características únicas. Este trabalho foca no estudo do reservatório *bootstrap*, uma solução amplamente utilizada em aplicações aeronáuticas devido à sua capacidade de manter a estabilidade do sistema em condições dinâmicas de operação. Apesar da sua relevância, há uma escassez de estudos e análises aprofundadas sobre esses tipos de reservatórios, incluindo sua modelagem dinâmica.

Objetivos

O objetivo principal deste trabalho de conclusão de curso é desenvolver um modelo matemático de um reservatório pressurizado *bootstrap* para aplicações em sistemas hidráulicos de aeronaves, com foco no controle de posição de superfícies de controle de voo e análise da dinâmica do reservatório. Para atingir esse objetivo, foram definidos os seguintes objetivos específicos:

- Revisão bibliográfica sobre os diferentes tipos de reservatórios pressurizados;
- Desenvolver modelos matemáticos para os componentes do sistema hidráulico, incluindo atuador, servo-válvula e reservatório *bootstrap*;
- Aplicar a metodologia de dimensionamento de componentes proposta por Furst & De Negri (2002);
- Analisar o comportamento do sistema de controle de posição sob diferentes condições de carga.

Metodologia

A metodologia adotada incluiu a revisão bibliográfica dos principais tipos de reservatórios pressurizados e a utilização da metodologia de Furst & De Negri (2002) para dimensionar os componentes hidráulicos, garantindo o atendimento às exigências de desempenho dinâmico do sistema. Modelos matemáticos foram desenvolvidos para simular o

comportamento do sistema hidráulico, utilizando o software MATLAB/Simulink. A dinâmica do sistema foi analisada considerando o comportamento da pressão no reservatório, a posição do atuador de controle da superfície de voo e a resposta às entradas de comando da servo-válvula, que determinam a posição do atuador.

Resultados e discussões

Os resultados das simulações confirmaram que o reservatório *bootstrap* conseguiu manter a pressão estável na entrada da bomba, independentemente da posição do reservatório ou do volume disponível, validando a relação entre o raio das áreas do atuador e a pressão gerada no reservatório. O sistema foi projetado para um tempo de acomodação de 1 segundo, e os resultados das simulações mostraram um valor de 0,975 segundos, atendendo às especificações do projeto.

Além disso, foi possível estabelecer uma relação entre a pressão de alimentação, a razão entre as áreas do reservatório e a pressão resultante no reservatório. Essa abordagem permitiu dimensionar adequadamente o reservatório *bootstrap* para garantir o funcionamento estável do sistema hidráulico, mesmo sob condições operacionais dinâmicas.

Conclusão e trabalhos futuros

Os resultados obtidos demonstram que o modelo matemático desenvolvido para o reservatório *bootstrap* atende às exigências de sistemas hidráulicos de aeronaves, proporcionando controle de posição e pressão do reservatório estável. Embora os resultados tenham sido consistentes com as expectativas, estudos futuros devem incluir a validação experimental em bancada de testes para avaliar o desempenho do sistema em condições reais. Além disso, recomenda-se o estudo da integração do reservatório *bootstrap* em sistemas hidráulicos mais complexos.

Palavras-chave: Sistemas hidráulicos. Reservatório *bootstrap*. Reservatórios pressurizados. Simulação de sistemas hidráulicos.

ABSTRACT

As aircraft grew larger and more complex, the demand for more robust and efficient hydraulic systems became critical. To meet these demands, pressurized reservoirs such as air-pressurized, gas-pressurized, and bootstrap reservoirs were developed, each ensuring sufficient suction pressure at the pump inlet and stable performance under varying operational conditions. This bachelor thesis focuses on the bootstrap reservoir. The study investigates the design and simulation of a pressurized hydraulic system incorporating a bootstrap reservoir for aircraft applications, addressing pressure stability and position control of a flight control surface under dynamic conditions. A mathematical model was developed for the components, including the actuator, servo-valve, and bootstrap reservoir, to simulate the system's behavior. The methodology proposed by Furst & De Negri (2002) was applied to size the hydraulic components, such as the actuator and servo-valve, ensuring the system met the desired dynamic response and position control requirements. These requirements, including maximum step displacement, accommodation time, and load force, were confirmed in the simulation results. The system achieved stable reservoir pressure and precise position control, with an accommodation time of 0.975 seconds, meeting the design specification of 1 second. The results aligned with the expected behavior of the bootstrap reservoir, confirming its effectiveness in maintaining system stability and ensuring position control under dynamic conditions. These findings lay the foundation for future experimental validation and the potential integration of the bootstrap reservoir dynamics into more complex hydraulic systems.

Keywords: Hydraulic systems. Bootstrap reservoir. Pressurized reservoir. System simulation.

FIGURES LIST

TABLES LIST

LIST OF ABBREVIATIONS

EDP – Engine Driven Pump

EMI – Electromagnetic Interference

FBW – Fly-By-Wire

FCS – Flight Control System

HIRF – High Intensity Radiated Field

LASHIP – Laboratory of Hydraulic and Pneumatic Systems

MFCS – Manual Flight Control System

PTS – Power Transfer System

PTU – Power Transfer Unit

SHA – Servo Hydraulic Actuator

UFSC – Federal University of Santa Catarina

LIST OF SYMBOLS

GREEK ALPHABET

β	Bulk modulus	[Pa]
γ	Heat capacity ratio	[1]
ξ	Damping factor	[1]
ω	Pump rotation	[rad/s]
$\omega_{n\,v}$	Valve natural frequency	[rad/s]
ω_n	Natural frequency of the system	[rad/s]

LATIN ALPHABET

A_A	Area of actuator chamber A	[m²]
A_B	Area of actuator chamber B	[m²]
A_{acc}	Accumulator area	[m²]
A_p	Relief valve area subjected to the pressure force	[m²]
A_t	Relief valve opening outlet area	[m²]
A_{ori}	Relief valve inlet area	[m²]
A_T	Reservoir actuator area	[m²]
A_e	Equivalent actuator area	[m²]
A_S	Reservoir system actuator area	[m²]
A_{ratio}	Reservoir area ratio	[1]
B	Viscous friction coefficient	[N.s/m]
D	Pump displacement	[cm³]
F_{fr}	Friction force	[N]
F_L	External load force	[N]
f_v	Viscous friction coefficient	[Ns/m]
K_v	Valve flow rate coefficient	[$m^3/(sPa^{0.5})$]
$K_{v\,cat}$	Catalog valve flow rate coefficient	[$m^3/(sPa^{0.5})$]
K_{vin}	Valve leakage coefficient	[$m^3/(sPa^{0.5})$]
$K_{vin\,pilot}$	Valve pilot leakage coefficient	[$m^3/(sPa^{0.5})$]
$K_{P\,leak}$	Pump leakage coefficient	[$m^3/(sPa^{0.5})$]
K_P	Proportional gain	[V/m]
K_i	Integral gain	[V/(m.s)]
M_T	Total moving mass of the reservoir	[kg]
M_{at}	Total mass in movement of the actuator	[kg]
M_{poppet}	Relief valve poppet mass	[kg]
p_A	Pressure in actuator chamber A	[Pa]
p_B	Pressure in actuator chamber B	[Pa]
p_{acc}	Hydraulic fluid pressure in accumulator	[Pa]
p_g	Gas pressure in accumulator	[Pa]
p_0	Accumulator initial pressure	[Pa]
p_{PA}	Pump pressure A chamber (suction chamber)	[Pa]
p_{PB}	Pump pressure B chamber (pressure chamber)	[Pa]
p_{rv}	Pressure relief valve	[Pa]
p_L	Load pressure	[Pa]

$p_{L\,vmax}$	Load pressure considering maximum velocity	[Pa]
Δp_T	Total pressure difference across the servo-valve	[Pa]
q_{VA}	Flow rate of actuator chamber A	[m³/s]
q_{VB}	Flow rate of actuator chamber B	[m³/s]
$q_{vin\,pilot}$	Pilot leakage flow rate	[m³/s]
$q_{V\,acc}$	Accumulator flow rate in/out	[m³/s]
$q_{Vv\,in}$	Flow rate into servo valve	[m³/s]
$q_{Vv\,out}$	Flow rate out of servo valve	[m³/s]
$q_{VP\,in}$	Flow rate in pump	[m³/s]
$q_{VP\,out}$	Flow rate out pump	[m³/s]
$q_{VP\,leak}$	Pump leakage flow rate	[m³/s]
$q_{VP\,cat}$	Pump catalog flow rate	[m³/s]
$q_{Vrv\,in}$	Flow rate in relief valve	[m³/s]
$q_{Vrv\,out}$	Flow rate out relief valve	[m³/s]
$q_{Vv\,in}$	Flow rate from the system to the servo valve	[m³/s]
$q_{Vv\,out}$	Flow rate from the servo valve to the reservoir	[m³/s]
t_s	Accommodation time	[s]
$U_c(s)$	Output signal	[V]
$U_n(s)$	Input signal	[V]
V_A	Volume of actuator chamber A	[m³]
V_B	Volume of actuator chamber B	[m³]
V_{A0}	Dead volume of the chamber A	[m³]
V_{B0}	Dead volume of the chamber B	[m³]
V_{acc}	Accumulator volume	[m³]
V_g	Gas volume in accumulator	[m³]
V_0	Accumulator initial volume	[m³]
V_{P0}	Dead volume of pump piston	[m³]
V_{PA}	Pump volume A chamber (suction chamber)	[m³]
V_{PB}	Pump volume B chamber (pressure chamber)	[m³]
V_{rv}	Volume relief valve	[m³]
V_S	Reservoir system volume	[m³]
V_{S0}	Dead volume of system chamber	[m³]
V_p	Piping volume	[m³]
V_T	Reservoir volume	[m³]
V_{T0}	Dead volume of reservoir chamber	[m³]
$v_{a\,maxp}$	Maximum positive velocity	[m/s]
x_c	Actuator displacement	[m]
x_{rv}	Relief valve displacement	[m]
x_0	Relief valve pre-compressed length of the spring	[m]
x_R	Reservoir displacement	[m]
x_{st}	System steady-state displacement	[m]

SUMMARY

1. INTRODUCTION

1.1. CONTEXTUALIZATION

The hydraulic system is regarded as a separate subsystem of an aircraft structure, however it is, in fact, an inseparable part of many other subsystems, such as the landing gear, flight control surfaces and braking system. In modern aircraft, nearly all power stages of actuators are hydraulic. For instance, a 4th generation fighter has more than ten independent flight control surfaces, each actuated by electrohydraulic actuators based on flight control system commands (AALTONEN, 2016).

Hydraulic systems are crucial for the operation of aircraft. They are responsible for the performance and reliability of various subsystems. Hydraulic reservoirs, an essential part of these systems, store hydraulic fluid and ensure a constant supply to the pumps. These reservoirs also receive fluid from the actuators of the aircraft, store it, and then allow it to flow into the suction side of the hydraulic pumps. To this matter, it is necessary that the reservoir provides positive inlet to the pump to avoid cavitation and ensure efficient pump operation (XIAO *et al*., 2013).

The most common and modern flight control system is the Fly-by-Wire system, where instantaneous load on the hydraulic system is not solely determined by pilot commands and maneuvers. Instead, the movements of flight control surfaces are determined by the current flight state, load, and environmental conditions, rather than being directly dependent on pilot commands (TERRY, 1998; TUTTLE *et al*., 1990).

The aircraft reliability is highly dependent on the reliability and robustness of the hydraulic system. Hydraulic pumps, reservoirs, and their associated components are fundamental to an aircraft's hydraulic system, making them the most critical elements of the system (AALTONEN, 2016).

Specifications for hydraulic system configurations are outlined in standards like SAE AS 5440, while reliability and damage tolerance are governed by standards such as MIL-F-8785. Fixed-wing aircraft must maintain maneuverability even with damage to one or two components or circuits. To meet these requirements, hydraulic systems typically feature at least two separate pumps powering different systems, with the capability to cross-connect when needed. In multi-engine aircraft, each pump is driven by a different engine, ensuring redundancy (MARÉ, 2017; AALTONEN, 2016).

Hydraulic reservoirs in aircraft hydraulic systems differ from those in mobile hydraulic applications. Aircraft reservoirs are designed to be as small and lightweight as possible to meet weight requirements. They must also operate reliably under extreme conditions, including high altitudes, wide temperature ranges, and varying pressures. Additionally, aircraft reservoirs are pressurized to ensure a consistent fluid supply to the hydraulic pump, regardless of the aircraft's orientation, acceleration, or other dynamic conditions, thereby preventing cavitation on the pump inlet side. There are several different ways to achieve reservoir pressurization: Air charge using engine bleed air, inert gas (nitrogen) charge and bootstrap reservoir (AALTONEN, 2016).

The pressurized reservoir concept dates back to at least 1958 when Michael (1962) combined a reservoir and accumulator to pressurize the oil for hydraulic pumps in aircraft systems. In 1962, Dick (1962) developed a gas-charged accumulator-reservoir unit. Xiao *et al.* (2013) analyzed the common faults in aircraft hydraulic reservoirs and proposed improvements to enhance their reliability and performance. Aaltonen (2016) investigated pump supply pressure fluctuations and the interaction between bootstrap reservoirs and hydraulic pumps in aircraft systems. Tao (2016) focused on bootstrap reservoir pressurization systems for civil aircraft hydraulic supplies. Xu *et al.* (2021) examined asymmetrical wear in aircraft bootstrap reservoirs, analyzing issues related to sealing types and supporting structures.

To gain a deeper knowledge of the pressurized reservoir's role and performance in an aircraft's hydraulic system, it is essential to study the system and component-level phenomena encountered during actual flight operations. Traditional methods, such as test benches, functional simulators (iron birds) or test flights, present challenges related to cost, equipment availability, and risk. Test flights are complex and expensive, while functional simulators are often not readily available.

To address these limitations, a simulation model will be developed to systematically analyze the behavior of the pressurized reservoir under various operating conditions. This approach will provide valuable insights into the reservoir's performance without the need for extensive physical testing, offering a more cost-effective and efficient means of understanding its function and potential issues.

1.2. OBJECTIVES

1.2.1. Main objectives

The objective of this bachelor thesis is to develop a mathematical model of a pressurized bootstrap reservoir in order to control the aircraft flight control surfaces and analyze the reservoir dynamics.

1.2.2. Specific objectives

In order to achieve the main objective of this bachelor thesis, aiming the use of pressurized hydraulic reservoir for application in aircraft, the following specific objectives were defined:

- Literature review on the different types of pressurized reservoirs;
- Develop the necessary mathematical models to simulate the hydraulic position control system with a bootstrap reservoir;
- Analyze the behavior of the control surface position system, including the effect of load forces;
- Apply the methodology introduced by Furst & De Negri (2002) for sizing hydraulic components in valve-controlled hydraulic positioning systems.

1.3. BACHELOR THESIS OUTLINE

The structure of the bachelor thesis manuscript is outlined as follows: Chapter 2 provides a literature review of the main flight control systems and the pressurized reservoir. In Chapter 3, a mathematical model of position control for control surface using a servo hydraulic actuator with a pressurized reservoir is developed. Chapter 4 applies the design procedure for sizing hydraulic positioning system components introduced by Furst & De Negri (2002) to select components for the hydraulic system, namely the actuator and the servo-valve. Chapter 5 shows the simulation results for a step reference input and for a right aileron position for an aircraft maneuver. Chapter 6 presents the conclusions of the bachelor thesis and future researches and Chapter 7, the references.

2. LITERATURE REVIEW

2.1. FLIGHT CONTROL SYSTEMS AND CONTROL SURFACES

2.1.1. Introduction

In aircraft, the Flight Control System (FCS) is considered one of the most important systems because it directly influences performance and reliability. The flight control needs to carry out the control of aircraft flight path, altitude, airspeed, aerodynamics configuration, and others. According to Wang *et al.* (2016), the flight control system (FCS) is a mechanical/electrical system that transmits control signals and drives surfaces to achieve scheduled flight according to the pilot's commands.

Since the advent of heavier-than-air aircraft, pilots have used mechanical systems to operate control surfaces, known as the manual flight control system (MFCS), which functions without power. These systems generate the power needed to move aircraft parts through control devices such as the control stick. This power is transmitted mechanically via rods, levers, pulleys, cables, etc., or hydrostatically for non-assisted braking systems, involving a master cylinder, tubes, and cylinder receptors (MARÉ, 2017). Figure 2.1 illustrates the aircraft's purely mechanical control system, where a steel cable or rod drives the control surfaces.

Figure 2.1 - Mechanical flight control system.

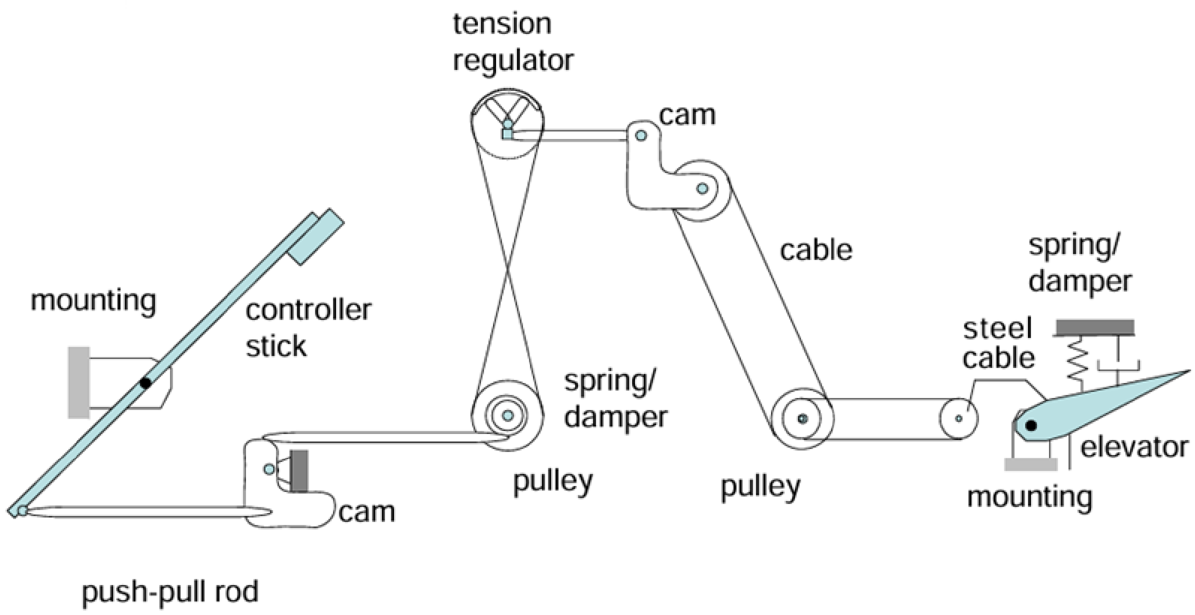

Source: BUDIYONO *et al*. (2006).

When the pilot wants to move the elevator, pulling the control column physically moves the elevator, which controls the aircraft's pitch. By moving the elevator up or down, the pilot can raise or lower the aircraft's nose, respectively. During this period, designers focused on minimizing friction, clearance, and elastic deformation within the transmission system to ensure optimal performance (WANG *et al*., 2016).

To change direction, such as making a right turn, the pilot adjust the ailerons of the aircraft. This adjustment, however, introduces adverse yaw, which is countered by the rudder. In a manual flight control system (MFCS), the ailerons and rudder were mechanically attached to each other, ensuring coordinated movement to manage adverse yaw. However, in modern aircraft with advanced technology, this coordination is controlled by the main aircraft computer. The computer automatically adjusts the rudder in response to aileron inputs, optimizing the aircraft's stability and control during maneuvers (HUNSAKER *et al*., 2020).

As aircraft became larger, heavier, and faster, the forces required for actuation increased, making it challenging for pilots to move the control surfaces against aerodynamic forces. In response, the aircraft hydraulic system had to evolve to keep up with these aerodynamic forces, enabling pilots to maneuver the aircraft. To overcome this situation, in the 1940s, hydraulic boosters were developed and introduced in the aircraft. Figure 2.2 shows the hydraulic booster, where geometry of the linkages determines the relationship between the pilot's input and the movement of the hydraulic booster, with lever arm lengths adjusting force. The linkages maintain a direct connection for feedback, while the hydraulic booster amplifies the input force using hydraulic pressure (WANG *et al*., 2016).

Figure 2.2 - Mechanical actuator with hydraulic booster.

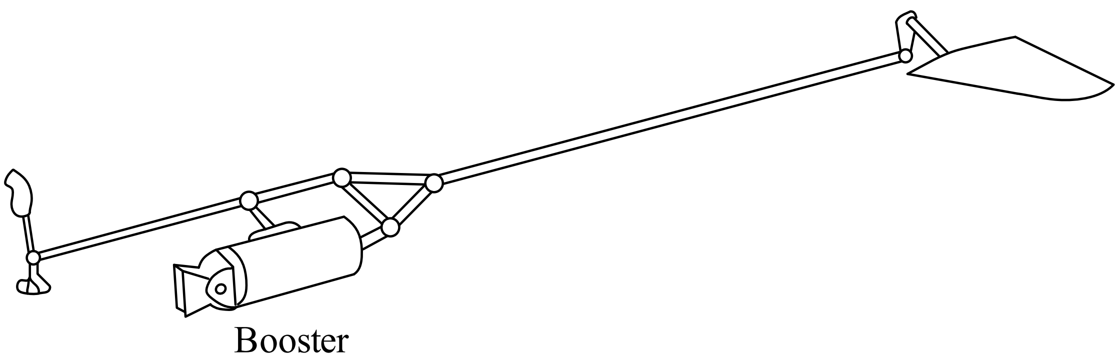

Source: Adapted from WANG *et al*. (2016).

This type of control system is called Power Assisted Flight Control System. The hydraulic booster is designed to enhance the performance of the existing mechanical components. These actuators assist the pilot by providing additional force to move the control surfaces. In the event of failure or malfunction, the pilot retains control of the aircraft. This redundancy allows for continued safe operation of the aircraft even if the hydraulic system becomes inoperative (BUDIYONO *et al*., 2006).

Since the 1950s, centralized hydraulic supply systems have been employed to power actuation systems for surface movement. These systems primarily utilize hydraulic fluids to transmit and distribute forces to various components that require actuation, particularly the control surfaces that govern the aircraft's maneuverability (WANG *et al*., 2016).

In order to exemplify the application of the hydraulic systems in aircraft, Figure 2.3 shows a simplified hydraulic circuit.

Figure 2.3 - Aircraft simplified hydraulic system.

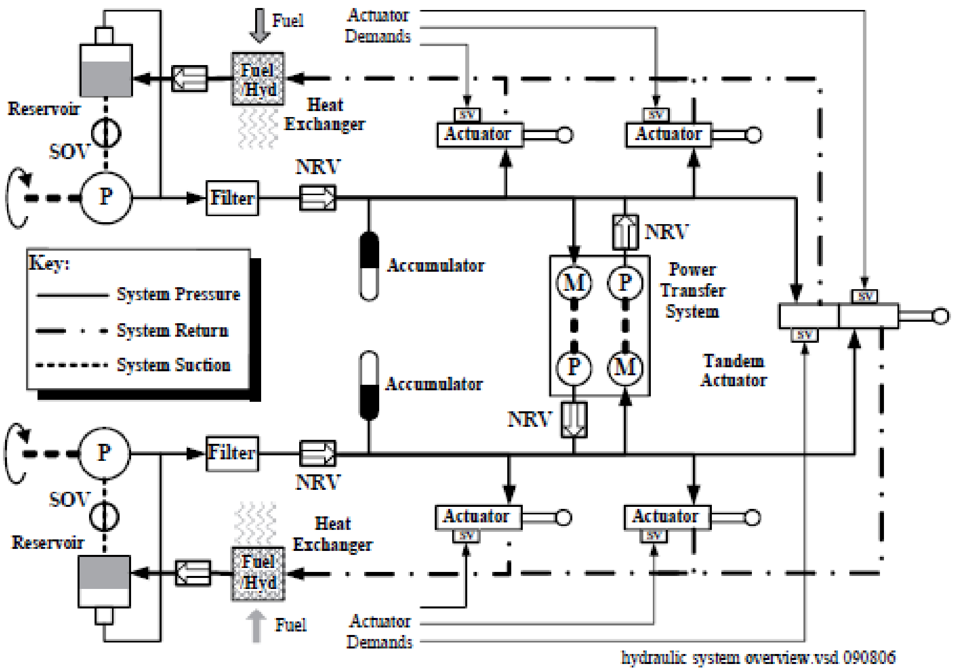

Source: MOIR & SEABRIDGE (2008).

As can be seen in Figure 2.3, more than two independent hydraulic systems operate autonomously to meet aircraft safety standards. In the event of failure of one of the hydraulic systems, the power transfer system (PTS) is activated. Thanks to this system, it is possible to exchange power between circuits without any fluid exchange. Filters remove fluid contaminants, accumulators release stored pressure as needed and can operate as backup flow rate source, the heat exchanger dissipates heat from returning oil using a fuel heat sink, reservoir stores hydraulic fluid, servo valves regulate distribution of the flow rate and actuator moves control surfaces (WANG *et al*., 2016).

The power generated by the aircraft engine drives hydraulic pumps that supply hydraulic power to the actuators, which in turn control the flight control surfaces. The Airbus A340 is equipped with three redundant hydraulic systems (Figure 2.4), each capable of independently controlling the aircraft. This redundancy is crucial for ensuring operational reliability and safety, allowing the aircraft to maintain control even in the event of a hydraulic system failure. Each hydraulic system operates with its own set of pumps, reservoirs, and distribution networks, providing backup capability in case of a system failure. This design reinforces the aircraft's ability to manage critical systems such as control surfaces, landing gear, and brakes under challenging conditions or failures, thereby ensuring continuous flight safety (TRAVERSE *et al*., 2004).

Figure 2.4 - Structure of an aircraft hydraulic system.

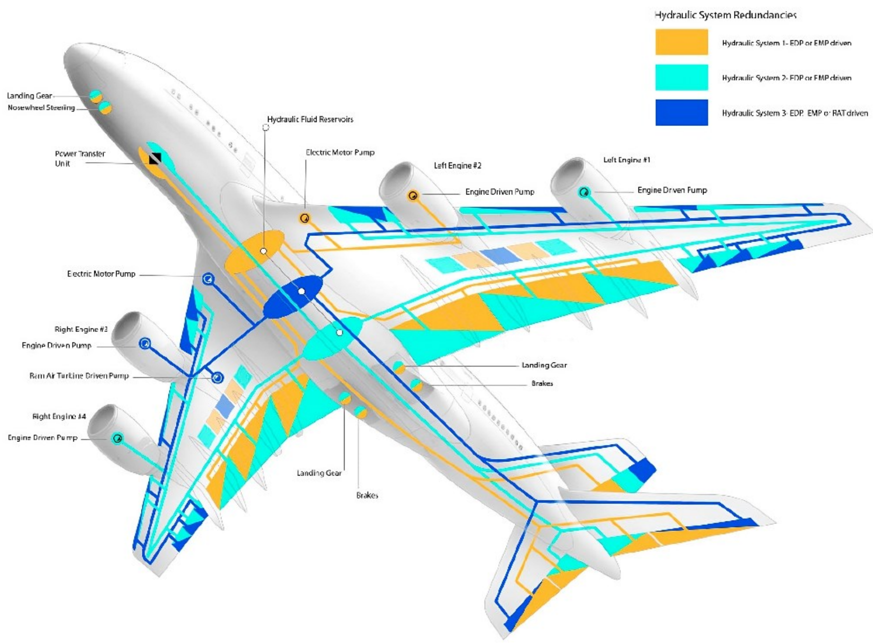

Source: (SHEN & ZHAO, 2023).

Around the 1980s, the shift from centralized to decentralized hydraulic systems in aircraft began. This transition was driven by advancements in miniaturized electro-hydraulic pumps and smart actuators, which allowed for more efficient, reliable, and lighter systems by distributing multiple small pumps and actuators throughout the aircraft instead of relying on a single centralized system (FORD, 1998).

As flight range and duration increased, it became necessary to develop and implement an automatic control system to improve the flight performance and reduce pilot fatigue. Then, the electrically signaled hydraulic powered actuator emerged to drive the aircraft control surfaces, known as Fly-by-Wire (FBW). The first commercial aircraft to feature this electrical system was the Concorde, designed and installed by Aerospatiale (ORLEBAR, 2010). This was an analogue system, that copied the stick commands onto the control surfaces while adding stabilizing terms. In the 1980s, the first generation of civil aircraft with digital technology came, including the Airbus A310 (WANG *et al*., 2016; TRAVERSE *et al*., 2004; MOIR & SEABRIDGE, 2008).

According to Moir & Seabridge (2008), all front-line fighters employ Fly-by-Wire systems. This system provides artificial stability to unstable aircraft and enhance aircraft handling, thereby improving pilot performance. Additionally, Fly-by-Wire systems save weight and significantly reduce structural loading by limiting demands as needed, however at the expense of functional complexity within the flight control software. These advancements are made possible by progress in microelectronics and actuation techniques.

The term Fly-by-Wire initially referred to the use of electrical signaling instead of mechanical linkages to transfer the pilot's commands to the flying control actuators. This technology was initially experienced during the 1970s in the Concorde program, where the system provided electrical signals directly proportional to the displacement of the pilot's control movements, without any control enhancement (FAVRE, 1994).

At the start of the 1980's, the development of the A320, A321, A330, and A340 aircraft revolutionized FBW by incorporating control laws that provided stability augmentation and flight envelope limiting. In modern Fly-by-Wire systems, control surfaces are no longer directly linked to pilot inputs, which eliminates the need for mechanical linkages. Instead, electronic signals from the pilot's commands are processed by a computer system, which then adjusts the control surfaces accordingly. Additionally, direct feedback on aerodynamic characteristics is not transmitted back to the pilot. Rather, instrument panels display this critical information, such as airspeed, altitude, pitch and roll, and vertical speed (FAVRE, 1994). The Fly-by-Wire control system is shown in Figure 2.5.

Figure 2.5 - Fly-by-Wire control system.

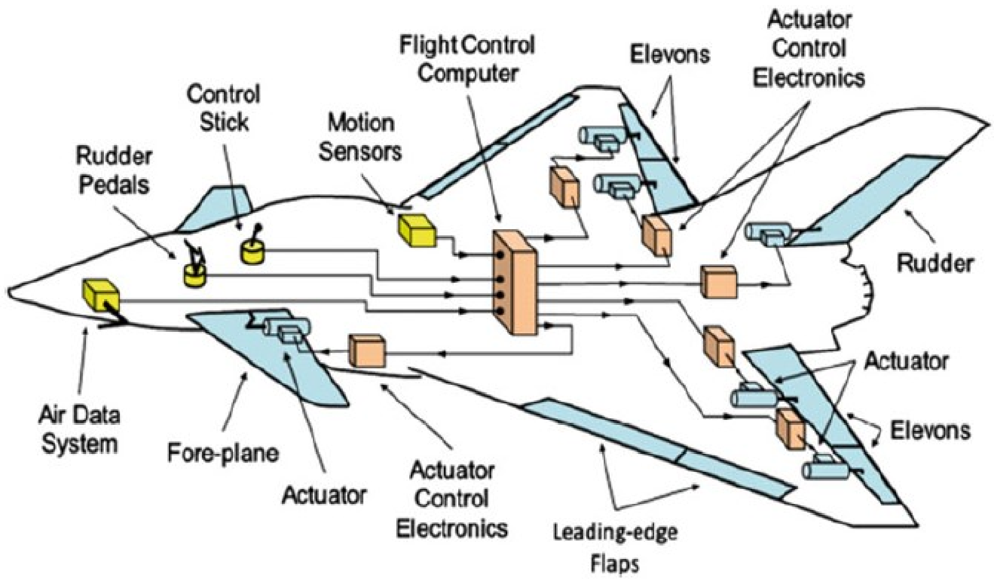

Source: COLLINSON (2023).

Flight envelope refers to the specific range of flight conditions within which an aircraft can operate safely and efficiently. These conditions typically include factors such as airspeed and load factor or altitude, and they define the operational limits and capabilities of the aircraft in terms of its performance, stability, and control. Through the implementation of control laws, certain maneuvers are limited to prevent exceeding operational limits, improving the aircraft safety (FIELDING, 2001).

According to Collinson (2023), control laws refer to the algorithms that relate control surface demands to the pilot stick commands, various motion sensor signals, and the aircraft altitude, speed, and Mach number. The primary objective of flight control laws integrated into a Fly-by-Wire system is to enhance the stability, control, and flight envelope protections. In a FBW system, computers process airspeed, inertial data, and aircraft state information to design control laws that translate pilot stick inputs into specific control commands. The control commands are continuously compared with real-time sensor data representing the aircraft actual state to ensure that the aircraft responds accurately to pilot inputs and maintains safe and stable flight conditions.

The advantages of this system are, based on Collinson (2023):

- Total elimination of complex mechanical control runs and linkages;

- The interposition of a computer between pilot's commands and the control surface actuators increases reliability and safety of the aircraft.

However, Garg *et al*. (2013) highlighted that some disadvantages are:

- Susceptibility to electromagnetic interference (EMI);
- High intensity radiated field (HIRF).

In the Fly-by-Wire system, the pilot operates the controls, and these inputs are transformed into electronic signals. These signals are then processed by the flight control computer and sent to the actuators. The actuators are responsible for moving the aircraft's control surfaces to achieve the desired control actions commanded by the pilot. This integrated process ensures responsive control of the aircraft (MOIR & SEABRIDGE, 2008).

The aircraft control system includes several different flying control surfaces, comprehending primary and secondary control surfaces. The primary control surfaces are essential for controlling an aircraft movement: the ailerons control roll, the elevators control pitch, and the rudder controls yaw. The secondary flight control surfaces, including slats, flaps, and spoilers, enhance the aircraft's performance and control: slats improve lift at lower speeds, flaps increase lift and drag for better control during takeoff and landing, and spoilers reduce lift and increase drag to assist in descent and braking (WANG *et al*., 2016). Figure 2.6 shows the main aircraft control surfaces.

Figure 2.6 - Control surfaces of a commercial aircraft.

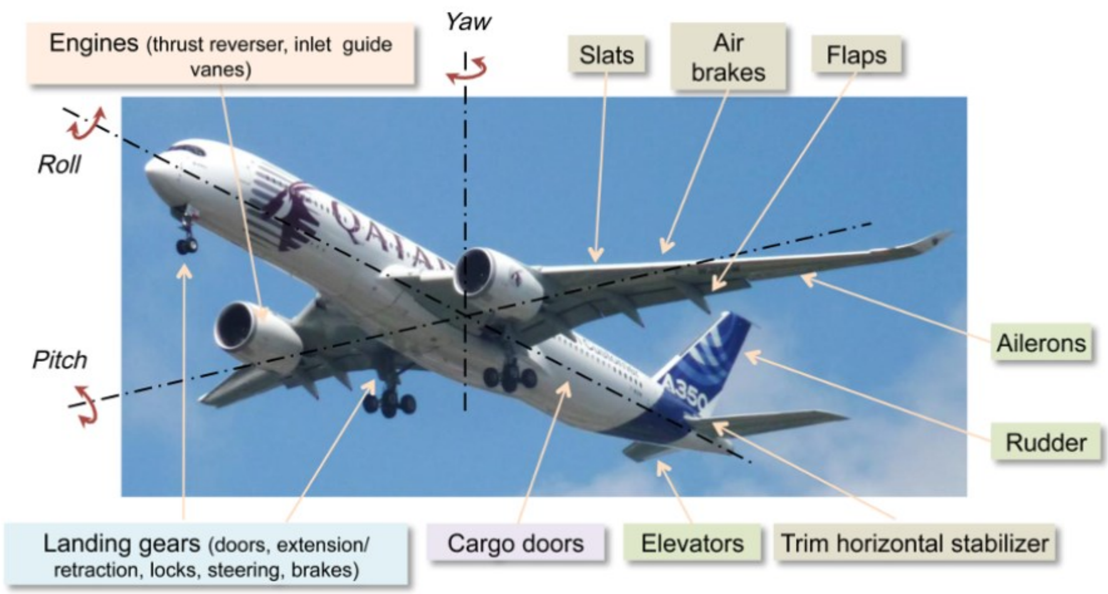

Source: (MARÉ, 2016).

According to Wang *et al* (2016), the interface between the flight control system and hydraulic systems is the actuation system. Hydraulic-powered actuators are connected to the control surfaces and are driven by the hydraulic power supply system. A hydraulic power supply system consists of an engine-driven pump (EDP), a power transfer unit (PTU), a hydraulic-driven generator, a hydraulic power package, a reservoir, an accumulator, a control valve, as shown in Figure 2.7.

The hydraulic reservoir is pressurized to ensure fluid is adequately forced into the pump, especially at high altitudes where atmospheric pressure decreases. This pressurization can be achieved using regulated bleed air from the pneumatic/bleed air system, a bootstrap reservoir, or an accumulator gas type bootstrap reservoir. Each hydraulic system has its own pressurized reservoir to prevent cavitation and ensure sufficient fluid is available under all demand conditions (WANG *et al*., 2016; MOIR & SEABRIDGE, 2008).

Figure 2.7 – Components of an aircraft hydraulic power supply system.

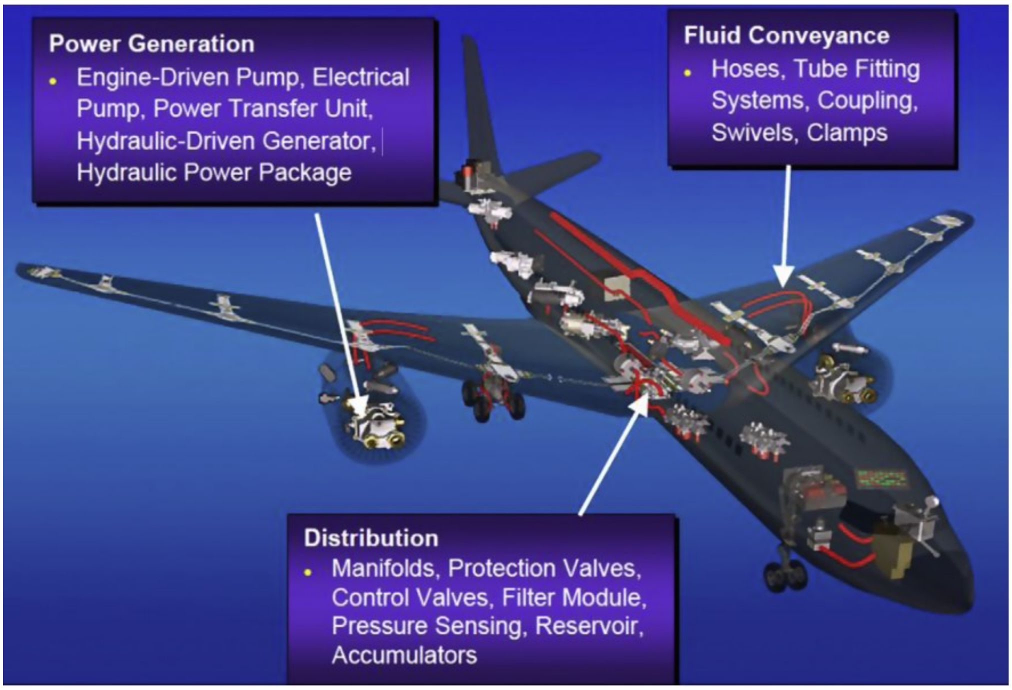

Source: (WANG *et al*., 2016).

2.2. AIRCRAFT HYDRAULIC RESERVOIR

In 1958, the first pressurized reservoir invented was a combination of a reservoir, accumulator and relief valve to pressurize the oil for hydraulic system pumps on missile installations, where positive oil pressure needs to be maintained on the suction side of the hydraulic pump in the system (MICHAEL, 1962). In 1962, Dick (1962) invented a gas-charged accumulator-reservoir unit, with a gas chamber relatively large, which allowed the accumulator pressure to remain substantially constant as the accumulator discharges. In both these solutions, the gas in the accumulator chamber exerts force in the reservoir. This force pressurizes the fluid in the reservoir and, since the cross-sectional area is much greater than the accumulator chamber, the reservoir pressure will be considerably less than the accumulator pressure. This construction can be seen in Figure 2.8.

In this figure, the black circle indicates the moveable barrier, the green circle denotes the fluid ports, and the orange circle highlights the chambers. Gas port (38) is used to introduce pressurized gas into the gas chamber (37), thereby pressurizing it. Pressurized fluid from the system enters through port (36) and is stored in accumulator chamber (35). The reservoir chamber is marked as (26). The force exerted by gas chamber (37) on case (16) pushes it to the right, thereby pressurizing the hydraulic reservoir.

Figure 2.8 - Gas charged accumulator-reservoir unit.

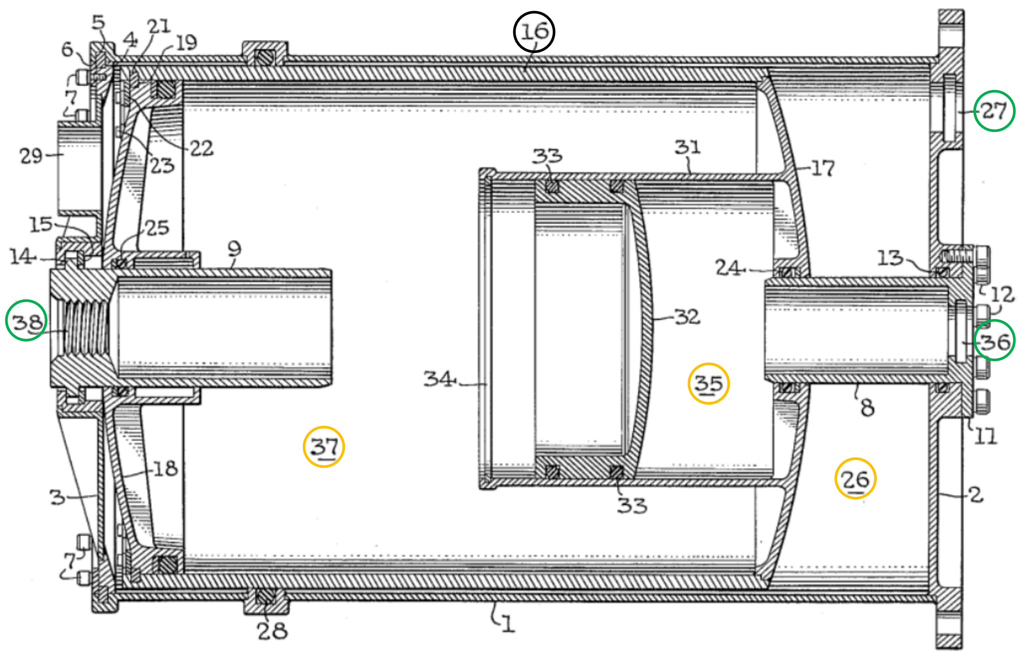

Source: Adapted from (DICK, 1962).

In 1987, Gooden (1985) developed the first bootstrap reservoir, which replaced the accumulator diaphragm with a piston to exert force within the reservoir chamber. This design, shown in Figure 2.9, includes a passageway (17) that connects to the discharge side of the pump and leads into annular chamber (33), which functions as the high-pressure chamber. The piston applies force to move towards flange (29), thereby pressurizing the low-pressure chamber (32).

Figure 2.9 - Reservoir device of the bootstrap type.

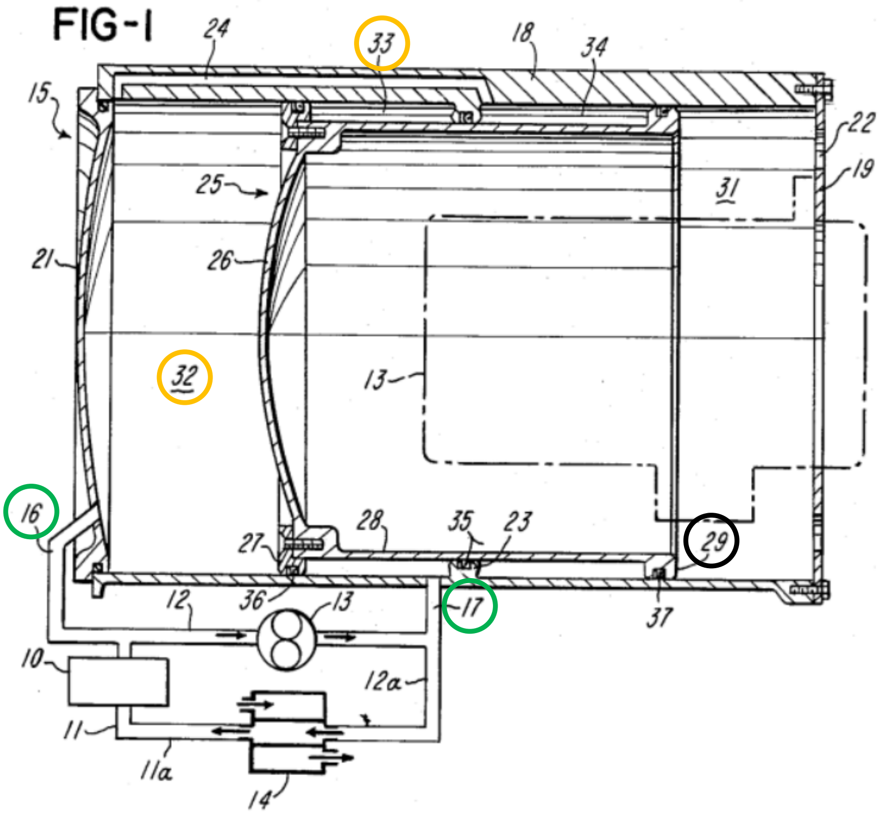

Source: Adapted from (GOODEN, 1985).

According to the Bureau of Naval Personnel (1951), the primary function of a hydraulic reservoir is to meet the operational demands of the hydraulic system and to replenish any fluid lost through leakage. These reservoirs are typically positioned at the highest point in the system to ensure that gravity assists in maintaining the pump's readiness for operation, thus enhancing the efficiency of the aircraft hydraulic systems.

Aircraft hydraulic reservoirs are designed to minimize weight, with pressurization methods such as engine bleed air, inert gas (e.g., nitrogen), or bootstrap systems ensuring consistent fluid supply under dynamic flight conditions. These methods address the specific demands of commercial and military applications, as discussed by Aaltonen (2016).

The following sections review each method (bootstrap reservoirs, bleed air pressurization, and gas-charged accumulators) detailing their operational principles, advantages and disadvantages.

2.2.1. Bootstrap reservoir

According to Tao (2016) the bootstrap reservoir consists of two connected hydraulic actuators, that utilize supply pressure from the pressurized system to maintain adequate return pressure on the storage side of the reservoir, ensuring the pumps meet minimum suction pressure requirements during full flow conditions and restart scenarios. This reservoir can be observed in Figure 2.10.

Figure 2.10 - Typical civil aircraft hydraulic system bootstrap reservoir.

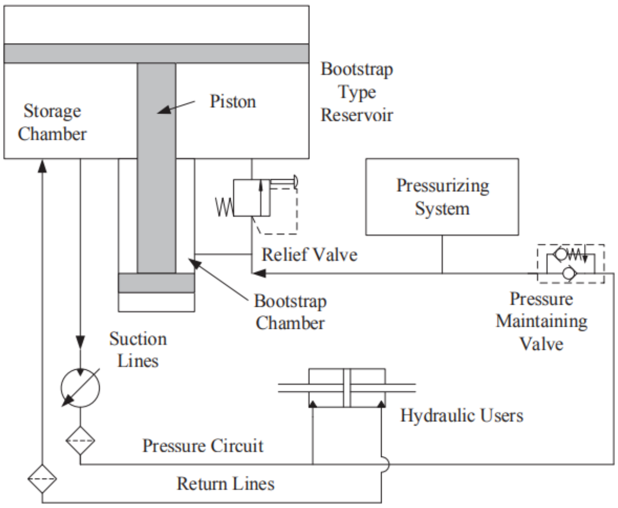

Source: (TAO, 2016).

The reservoir hydraulic schematic is shown in Figure 2.8. The reservoir utilizes a high-pressure chamber, known as the bootstrap chamber, which connects to both the pressurized system and the hydraulic system pressure circuit. It also includes a low-pressure chamber that connects to the pump suction and the return port of the aircraft's hydraulic system. The system pressure from the pump and the pressurized system acts on a small piston within the bootstrap chamber. This small piston is connected to a larger low-pressure piston, exerting sufficient force on the larger piston to pressurize the storage chamber volume and maintain the return pressure (TAO, 2016).

As stated by Xia *et al.* (2014), by adjusting the area ratio between the high-pressure and low-pressure chambers, the pressure in the low-pressure chamber can be defined and maintained. In operation, the balance of forces within the differential piston maintains the pressure in the pressurized reservoir. Even when there is a higher pressure due to the load, the reservoir pressure will remain constant. The self-pressurizing pump manages this process by controlling the differential piston to pressurize the oil in the low-pressure chamber, ensuring stable operation during aircraft maneuver.

Tao (2016) explains that when the pressurized system is unsuitable for the hydraulic system, the reservoir may not maintain adequate return pressure. Consequently, when starting the pump, the suction pressure could decrease to the saturated vapor pressure. This results in the release of entrapped air as free air, causing cavitation within the pump's suction port.

According to Maré (2017), this solution tolerance to load factors enables it to sustain consistent performance and pressure levels despite varying operational demands and external loads, making it particularly suitable for fighter aircraft and helicopters. While it eliminates the need for coupling with air systems typically used in air-pressurized reservoirs, the bootstrap reservoir requires additional devices, such as accumulators for maintaining pressurization after flight and bleeding mechanisms for system maintenance.

2.2.2. Bleed air pressurized reservoir

According to Waheed (2011), the function of any aircraft bleed air system is to extract compressed air from the engine and utilize it to power various aircraft systems. Engine bleed air on the Boeing 737 is typically sourced from the 5th and 9th stages of the engine compressor section.

In this type of reservoir, there is no physical separation between the air and the hydraulic fluid (free surface pressurized reservoir). The air used for pressurization, which comes into direct contact with the hydraulic fluid, must be filtered, decanted, and have its pressure controlled (MARÉ, 2017).

Based on Maré (2017), the advantages of this type of reservoir are:

- Facilitates separation of free gases by centrifuging the input fluid and then letting gravity led bubbles to the surface;

However, Maré (2017) also highlighted this reservoir disadvantages:

- Complex coupling between hydraulic systems and air systems;
- Necessity to implement particular construction features, such as anti-g walls to avoid sloshing under sideways acceleration, or walls enabling the essential hydraulic circuit to be fed in priority;
- Require a pre-pump to pressurize the fluid and remove air before it is transferred to the primary pump.

In the Boeing 737, there are three independent hydraulic systems: System A, System B, and a standby system, in Figure 2.11. The standby reservoir is connected to the System B reservoir for pressurization and servicing. The standby hydraulic system serves as a backup in case of pressure loss in System A and/or B. This system can be activated either manually or automatically and operates using a single electric alternating current motor pump. It powers the thrust reversers, rudder, leading edge flaps and slats (WANG *et al*., 2016).

Figure 2.11 - B737 NG Hydraulic reservoir pressurization system.

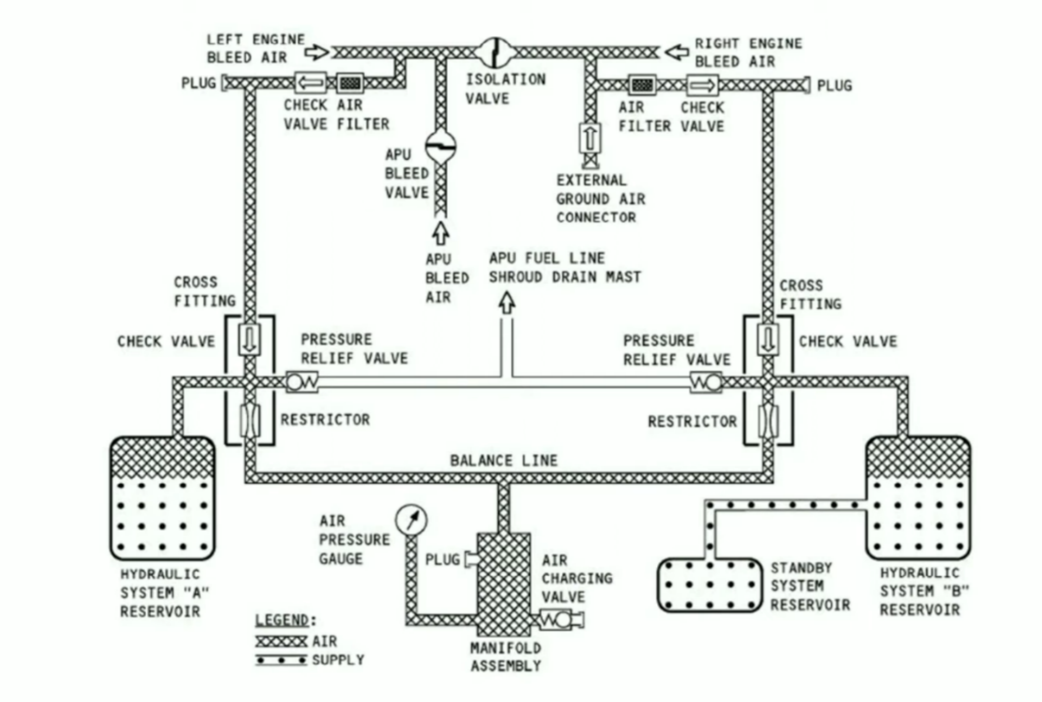

Source: Extracted from B737 NG Aircraft | Hydraulic Reservoir Pressurization System | Cross Fitting | Vent Line | Manifold (2020, 8min8s).

2.2.3. Accumulator gas type bootstrap reservoir

Accumulator gas type bootstrap reservoir presents a similar construction to the bootstrap reservoir. This reservoir uses the gas side of the accumulator to maintain the return pressure in the storage chamber and can also provide auxiliary flow to hydraulic users in normal flight profile (TAO, 2016). The Sukhoi Super Jet 100/SSJ-100 employs this reservoir type, depicted in Figure 2.12.

Figure 2.12 - Accumulator gas type bootstrap reservoir.

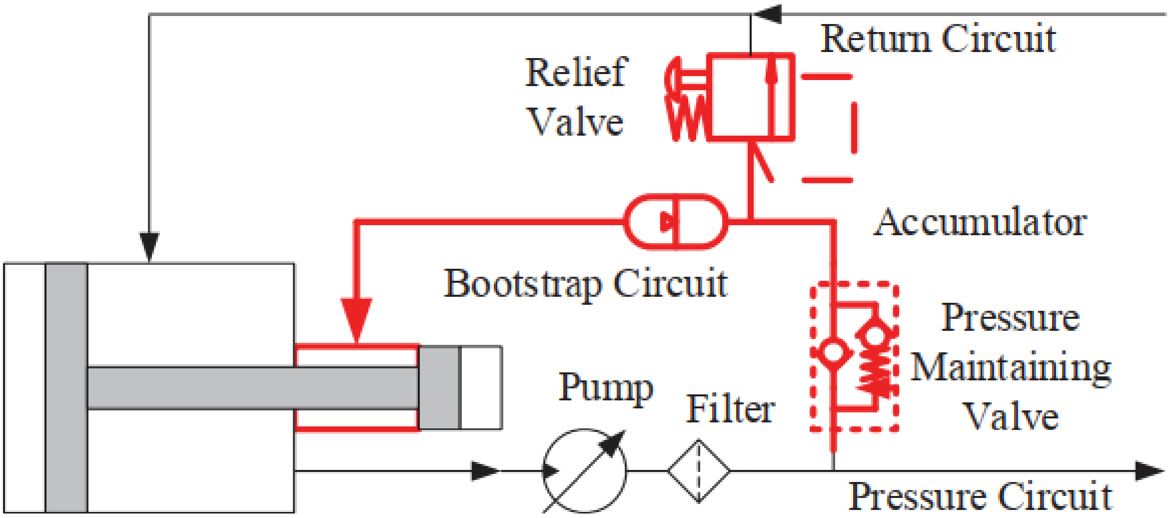

Source: (TAO, 2016).

According to Tao (2016), accumulator-based reservoirs offer advantages, such as extended pressure retention due to the pre-charged gas, which can sustain hydraulic function even with a complete fluid loss. This design slightly increases the effective size of the accumulator and eliminates the need for a fluid isolation valve. However, disadvantages include compromised seal performance at low temperatures (below -50°C), which may cause nitrogen to leak into the hydraulic fluid, as well as more frequent maintenance due to additional gas leakage points.

3. MODELING OF POSITION CONTROL FOR CONTROL SURFACE USING A SERVO HYDRAULIC ACTUADOR WITH A PRESSURIZED RESERVOIR

3.1. INTRODUCTION

In the Chapter 3, a mathematical model of the hydraulic system will be presented. The model here was developed based on the review from Nostrani (2015), Ledezma (2012), Cruz (2018), Rabie (2009) and Furst, De Negri (2002). Figure 3.1 shows the hydraulic circuit for the modeling of the system with a pressurized reservoir.

Figure 3.1 - Hydraulic system for position control using a servo hydraulic actuator with a pressurized reservoir.

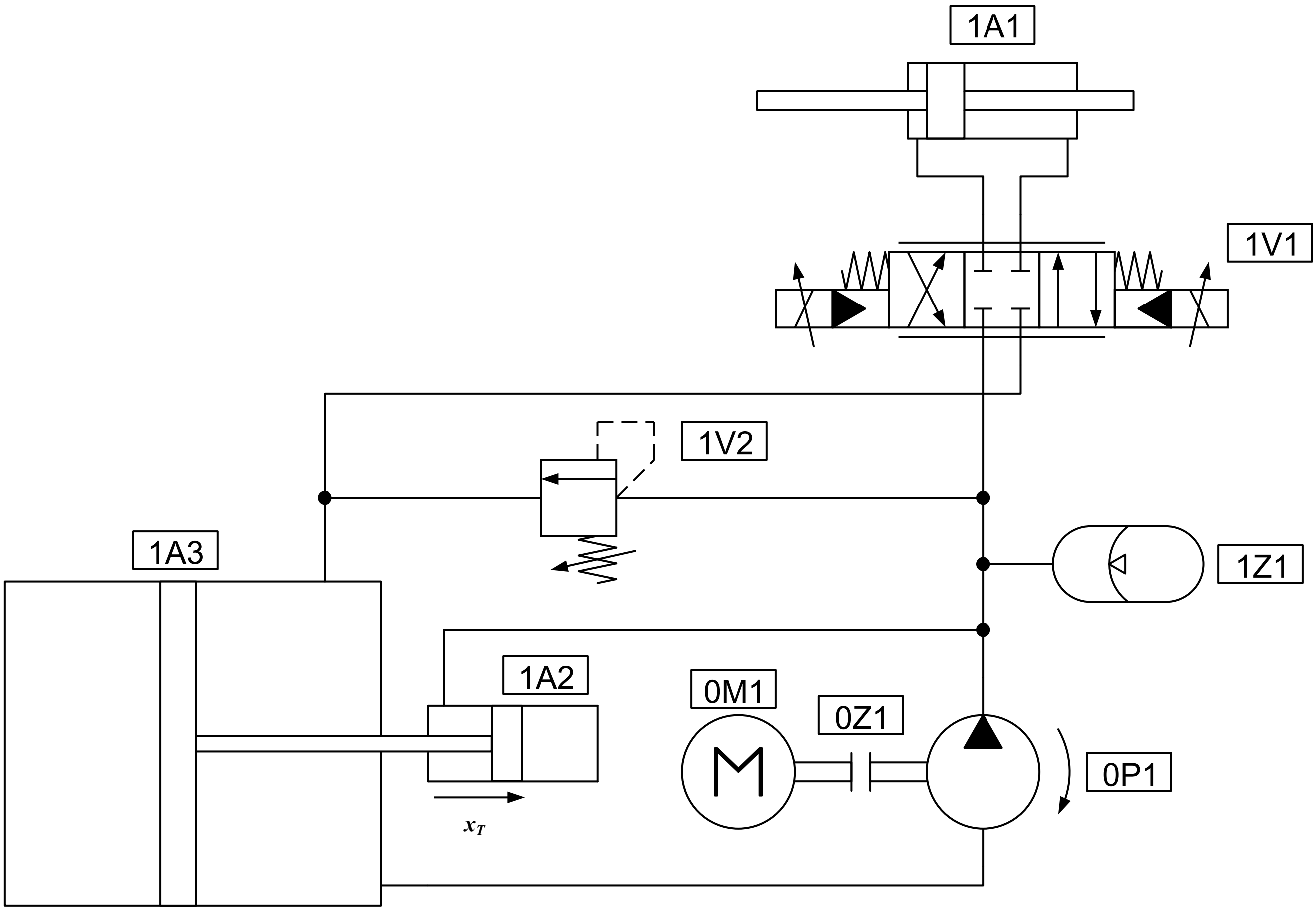

Source: By the author.

3.2. MODEL OF THE HYDRAULIC ACTUATOR

The dynamic behavior of the actuator can be described based on two main dynamics: hydraulic and mechanical, respectively. The hydraulic dynamics is based on the continuity equation, where pressure of the cylinder chambers can be obtained. The mechanical equation uses Newton’s second law, to describe the motion of the cylinder rod.

For this modeling, the cylinder is a double acting and symmetrical double rod. This solution is the most commonly adopted for steering landing gear and for primary flight control (MARÉ, 2016).

The actuator is responsible for performing the position control of a control surface in an aircraft. It operates to achieve the desired position, as directed by the aircraft's control surface system. Figure 3.2 shows the presence of these actuators on an aircraft.

Figure 3.2 - Airbus A380 Servo Hydraulic Actuator.

Source: van den BOSSCHE (2006).

The safety-critical systems in question operate in an active/standby failure mode, where multiple actuators are utilized for each flight control surface (CHURN *et al.*, 1998). According to Maré (2016), redundancy is employed to enhance a system's resilience against failure by duplicating system elements or incorporating backup (or standby) components. This ensures that the system maintains functionality even in the event of component failure.

3.2.1. Continuity equation applied to the actuator chambers

The Figure 3.3 shows the scheme of a symmetric double-acting actuator and its principal components.

Figure 3.3 - Schematic drawing of a symmetric double-acting actuator.

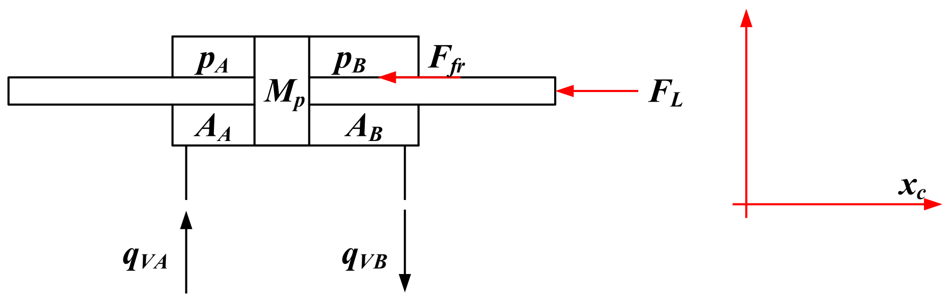

Source: By the author.

Based on Figure 3.3 and the principle of mass conservation (MERRIT, 1967), applying the continuity equation to chambers A and B of the actuator yields equations (3.1) and (3.2), respectively as follows. Internal leakage between chambers was not included in this model.

$$q_{VA} = \frac{\partial V_A}{\partial t} + \frac{V_A}{\beta}\frac{\partial p_A}{\partial t}, \tag{3.1}$$

$$-q_{VB} = \frac{\partial V_B}{\partial t} + \frac{V_B}{\beta}\frac{\partial p_B}{\partial t}, \tag{3.2}$$

where V_A and V_B [m³] are the volumes of chambers A and B, respectively, q_{VA} and q_{VB} [m³/s] the flow rates of chambers A and B, respectively. Additionally, p_A and p_B [Pa] are the pressures of chamber A and B, respectively. The bulk modulus is represented by β [Pa].

The volume change of chambers A and B in the actuator is influenced by the position of the actuator rod, requiring consideration of the dead volume due to the fluid confined within the connecting tubes between the valve and the cylinder. This relationship is described by equations (3.3) and (3.4).

$$V_A = V_{A0} + A_A x_c, \tag{3.3}$$

$$V_B = V_{B0} - A_B x_c, \tag{3.4}$$

where V_{A0} and V_{B0} [m³] are the dead volumes of chambers A and B, respectively, A_A and A_B [m²] the areas of chambers A and B, respectively, and x_c [m] is the actuator displacement.

3.2.2. Equation of motion applied to the hydraulic actuator

The dynamics of the cylinder rod can be obtained through Newton's second law, in Equation (3.5):

$$(p_A A_A) - (p_B A_B) - F_{fr} - F_L = M_{at}\ddot{x}_c, \tag{3.5}$$

where F_{fr} [N] the friction force, F_L the external load force [N] and M_{at} [kg] the actuator total mass in movement.

The friction force F_{fr} represented in Equation (3.5) incorporates contributions from the load, the actuator piston and the mechanical seals on the piston rod. The only nonlinear element in the equation is associated with friction forces, which generally depend on lubrication, wear between moving parts, seals, movement speed, system pressure, material, surface roughness, environmental conditions, and cylinder geometry (VALDIERO, 2005).

According to Valdiero (2005), friction dynamics significantly degrade system performance. These non-linear effects necessitate careful modeling and compensation strategies to mitigate their impact on actuator performance. The friction not only contributes to energy losses but also introduces variability in actuator behavior, particularly under transient conditions. This highlights the necessity of implementing robust control algorithms to account for such variabilities and maintain actuator precision.

Numerous studies (CANUDAS DE WIT *et al*., 1995; GOMES & ROSA, 2003; MAKKAR, DIXON, *et al*., 2005) have focused on developing a mathematical model to characterize the effects of friction. However, a universally accepted model has yet to be established. At the Laboratory of Hydraulic and Pneumatic Systems (LASHIP), the friction model proposed by Gomes & Rosa (2003), called the Variable Viscous Friction Model, has been widely adopted as a reference. In this model, the friction force is represented by Equation (3.6).

$$F_{fr} = f_v \frac{\partial x_c}{\partial t}, \tag{3.6}$$

where f_v [Ns/m] is the viscous friction coefficient.

The variable viscous friction model is an approach that accounts for the variation of the viscous friction coefficient as a function of the displacement speed between two solid surfaces. This model considers the non-linearity of viscous friction behavior and is particularly useful in situations where the displacement speed varies significantly.

The friction model used in this project is the non-linear Coulomb model, experimentally determined by Gonzalez (2012). The parameters of the friction model are shown in Table 3.1.

Table 3.1 - Parameters for friction model.

Polynomials	
Advance polynomial	[6.511×10^4 1.298×10^3 1.047×10^3 1.498×10^3]

Retract polynomial	[-7,6699 × 10^4 -3.049 × 10^3 -1.542 × 10^3]

Source: Gonzalez, 2012.

3.3. MODEL OF THE HYDRAULIC VALVE

Electrohydraulic servo valves are extensively utilized in both aerospace and industrial applications due to their reliability and exceptional performance (PLUMMER, 2016). These valves can continuously modulate flow in response to an input signal by employing a sliding spool as the control element (HUNT, VAUGHAN, 1996). They are essential components in closed-loop electro-hydraulic motion control systems (MERRIT, 1967; PLUMMER, 2016).

In servo valves, the spool overlap is typically very small, often 1% of the spool stroke or less (AMIRANTE *et al.*, 2014). This overlap results in a reduced dead zone, which enhances the valve response time, a crucial factor in aircraft applications where fast and precise control is needed. In contrast, proportional valves usually have larger overlaps, often exceeding 5% of the spool stroke.

A servo valve typically consists of a two-stage configuration, with a main stage (also known as the second stage) that houses the main spool responsible for metering flow, often through a four-way spool valve. The pilot stage (or first stage) serves as a hydraulic amplification system to control the main spool's movement (TAMBURRANO *et al.*, 2018). This configuration can be observed in Figure 3.4.

Figure 3.4 - Servo valve by MOOG.

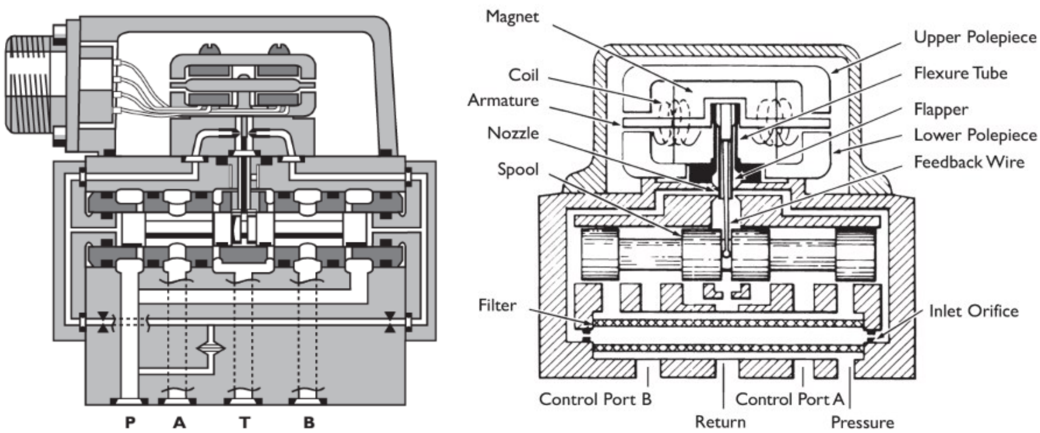

Source: Adapted from (MOOG, 2024).

One of the key parameters for specifying a servo valve is determining the total flow coefficient (K_v). This coefficient can be derived from the relationship between the control flow rate for a nominal input and a test pressure, considered as the nominal pressure. This relationship is typically provided in various valve manufacturer catalogs or can be extracted from flow versus input signal curves (FURST, DE NEGRI, 2002).

Due to manufacturing inaccuracies and the necessity for smooth sliding properties, leaks commonly arise between the spool and the sleeve of the valve. These leaks result in internal fluid leakage, which is undesirable yet unavoidable. In numerous spool valve applications, internal leakage serves as a significant factor influencing the design of hydraulic systems (D. GORDIĆ *et al.*, 2011).

Because of the internal leakage, a pressure difference occurs on hydraulic loads, influencing the system's behavior, e.g., inducing position errors in a P-controlled loaded actuator (ELLMAN, 1996).

The presence of clearance also facilitates the possibility of lubrication between elements with relative motion. However, in addition to internal leakage, clearance allows for the possibility of spool locking due to pressure imbalance or solid contaminants present in the fluid (LINSINGEN, 2013).

The pilot stage, often a small spring-loaded valve, regulates the flow to the main stage. Due to the high-pressure differentials and the need for precise control, a small amount of leakage is typical and, in some cases, permissible. The pilot stage is actuated by a torque motor, while the hydraulic amplification is obtained through a double-flapper nozzle, a deflector jet, or a jet pipe. There can be either mechanical feedback or electrical feedback depending on the application, with mechanical feedbacks more commonly used in aircraft (TAMBURRANO *et a*l., 2019).

3.3.1. Solenoid coil spool motion equation

The dynamics of the spool movement is characterized in Equation (3.7).

$$U_c(s) = \frac{{\omega_{n\,v}}^2}{s^2 + 2\xi\omega_{n\,v}s + {\omega_{n\,v}}^2} U_n(s), \tag{3.7}$$

where $U_c(s)$ is the output signal, $U_n(s)$ the input signal, ξ [1] the damping factor, $\omega_{n\,v}$ [rad/s] is the valve natural frequency.

3.3.2. Flow equation of the control orifice with internal leakage

In Figure 3.5, when a positive control signal U_c is applied to the solenoid, the spool shifts left (advance movement), connecting the supply pressure port to the actuator A chamber and linking the B chamber to the reservoir return line. With the supply pressure p_S being greater than the return pressure p_T, pressure in the A chamber p_A is greater than the pressure at the B chamber p_B of the actuator, resulting in a force available to move the actuator. When a negative control signal U_c is applied, the process reverses: the spool shifts right (retract movement), pressure at the B chamber p_B is greater than the pressure at pressure A chamber p_A, and the actuator moves to the other direction (DE NEGRI, 2001).

Figure 3.5 - Flow rate at valve working ports.

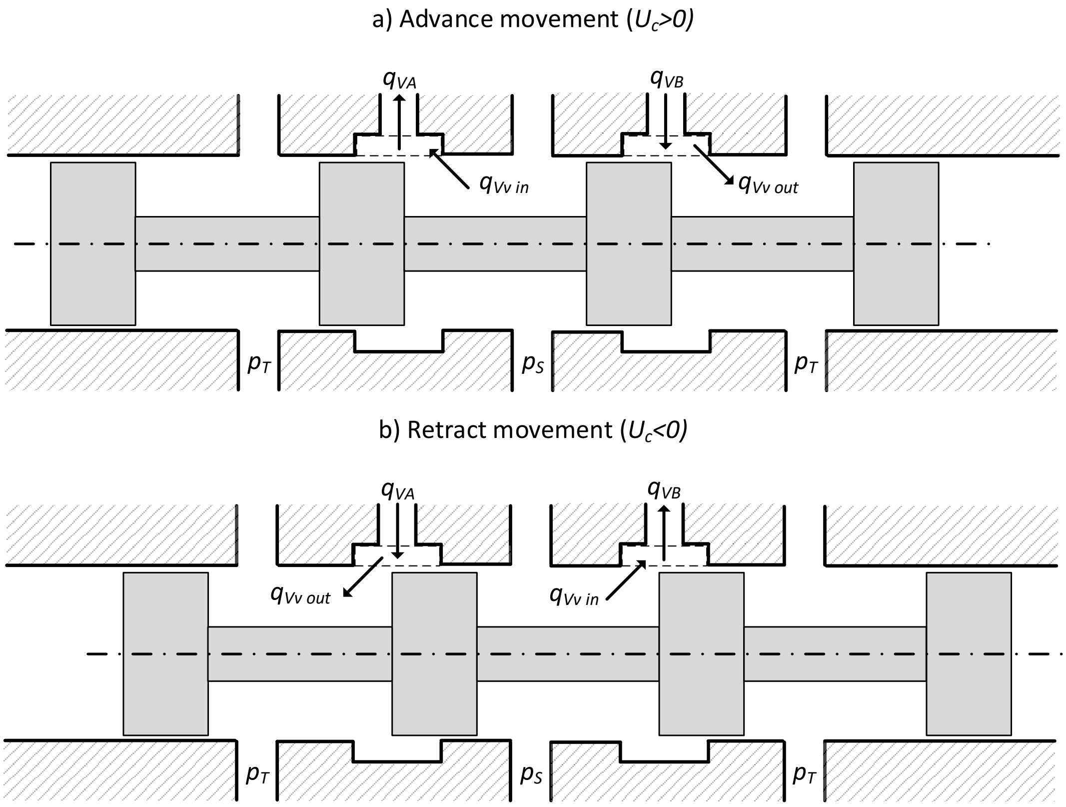

Source: By the author based on De Negri (2001).

The advance movement is governed by Equation (3.8), while for the retract movement, (3.9) is used. The hold, which is the closed center in the valve, is used to maintain the actuator in its current position (FURST, 2001).

$$U_c > 0 \qquad \begin{aligned} q_{VA} &= \left(K_v \frac{U_c}{U_n} + K_{vin}\right)\sqrt{p_S - p_A} - K_{vin}\sqrt{p_A - p_T}, \\ q_{VB} &= \left(K_v \frac{U_c}{U_n} + K_{vin}\right)\sqrt{p_B - p_T} - K_{vin}\sqrt{p_S - p_B}, \\ q_{Vv\,in} &= \left(K_v \frac{U_c}{U_n}\right)\sqrt{p_S - p_A}, \\ q_{Vv\,out} &= \left(K_v \frac{U_c}{U_n}\right)\sqrt{p_B - p_T}, \end{aligned} \tag{3.8}$$

$$U_c < 0 \qquad q_{VA} = -\left(K_v \frac{|U_c|}{U_n} + K_{vin}\right)\sqrt{p_A - p_T} + K_{vin}\sqrt{p_S - p_A}, \tag{3.9}$$

$$q_{VB} = -\left(K_v \frac{|U_c|}{U_n} + K_{vin}\right)\sqrt{p_S - p_B} + K_{vin}\sqrt{p_B - p_T},$$

$$q_{Vv\,in} = \left(K_v \frac{|U_c|}{U_n}\right)\sqrt{p_S - p_B},$$

$$q_{Vv\,out} = \left(K_v \frac{|U_c|}{U_n}\right)\sqrt{p_A - p_T},$$

where K_v and K_{vin} [$m^3/(sPa^{0.5})$] are the valve flow rate coefficient and valve leakage coefficient, respectively; $q_{Vv\,in}$ and $q_{Vv\,out}$ [m^3/s] represent the servo-valve inlet and outlet flow rates; and p_S and p_T [Pa] are the system and reservoir pressures.

3.3.3. Flow equation of the valve pilot leakage

The pilot leakage flow rate is calculated with Equation (3.10).

$$q_{vin\,pilot} = K_{vin\,pilot}\sqrt{p_S - p_T}, \tag{3.10}$$

where $q_{vin\,pilot}$ [m^3/s] is the pilot leakage flow rate, and $K_{vin\,pilot}$ [$m^3/(sPa^{0.5})$] is the valve pilot leakage coefficient.

3.4. MODEL OF THE HYDRAULIC ACCUMULATOR

Hydraulic accumulators in aircraft hydraulic systems serve multiple essential functions, including compensating for transient flow demands by storing energy, acting as backup energy sources for critical systems like brakes, maintaining pressure in isolated circuit parts to prevent issues like desorption and cavitation, and reducing pressure surges and water hammer effects to enhance overall system reliability and performance (MARÉ, 2016).

For the application on aircraft, the accumulator dampens pressure spikes in the pressure line, provide backup hydraulic power to the hydraulic fluid system, that can keep the actuator of control surface in the desired position in case of pump failure, and avoid cavitation when the system is shut down (PLAMONDON, 2020).

There are various types of accumulator designs, each suited to different applications. The most commonly available types are weight-loaded accumulators, spring-loaded accumulators, and gas-loaded accumulators. Among these, gas-loaded accumulators are the most widely discussed in the literature due to their versatility and operational characteristics. For aircraft applications, the most used type of accumulator is the gas-loaded, which are further subdivided into four categories, as shown in Figure 3.6, being (a) piston, (b) bladder, (c) diaphragm, (d) metal bellow.

Figure 3.6 - Different types of gas-charged accumulators.

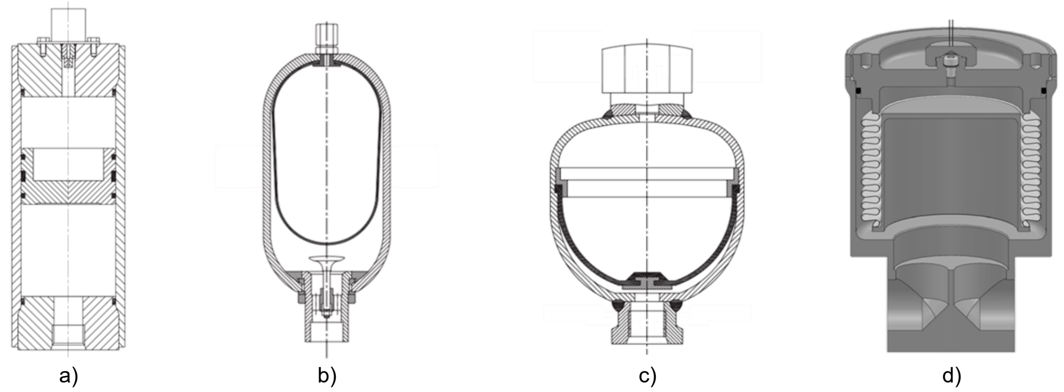

Source: By the author based on Vacca & Franzoni (2021).

Among these categories, hydropneumatic accumulators with metal bellows, first introduced on the Airbus A380, represent a significant advancement. These accumulators require no maintenance throughout the aircraft's lifespan because the metal bellows prevent gas diffusion. Additionally, by using helium instead of nitrogen, these accumulators can increase the restored volume by up to 44%, enhancing efficiency and reliability (DA COSTA; VILLENEUVE, 2004). Figure 3.7 shows a schematic model for the hydraulic accumulator.

Figure 3.7 - Schematic drawing for the accumulator.

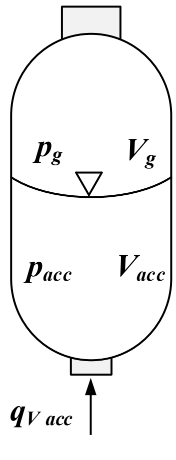

Source: By the author.

where $q_{V\,acc}$ [m³/s] is the flow in/out of the accumulator, V_{acc} and V_g [m^3] are the volume of the hydraulic accumulator and the gas volume in the accumulator, respectively, p_{acc} and p_g [Pa] the hydraulic fluid pressure in the accumulator and the gas pressure in the accumulator, respectively.

The development of the mathematical model was based primarily on Nostrani (2015), Rabie (2009) and Vacca & Franzoni (2021).

Applying the continuity equation in the accumulator yields the Equation (3.11).

$$q_{V\,acc} = \frac{\partial V_{acc}}{\partial t} + \frac{V_{acc}}{\beta}\frac{\partial p_{acc}}{\partial t}. \tag{3.11}$$

With the usage of the gas compression process equation, it is possible to correlate the gas pressure in the accumulator with the accumulator initial pressure and initial volume p_0 and V_0, respectively (RABIE, 2009). This relation is shown in Equation (3.12).

$$p_g^{\frac{1}{\gamma}} V_g = p_0^{\frac{1}{\gamma}} V_0, \tag{3.12}$$

where γ is the heat capacity ratio. In this project, the value of $\gamma = 1{,}4$, reflecting the nature of the adiabatic process. For an isothermal process, the heat capacity ratio should be $\gamma = 1$.

The gas volume can be calculated by the Equation (3.13), where V_0 [m³] is the accumulator initial volume.

$$V_g = V_0 - V_{acc}. \tag{3.13}$$

Deriving the Equation (3.13) in time, considering that the pressure in the accumulator is equal to the pressure of the gas ($p_g = p_{acc}$) and that the change ($\frac{dV_g}{dt} = -\frac{dV_{acc}}{dt}$), the Equation (3.14) can be obtained:

$$\frac{\partial V_{acc}}{\partial t} = \frac{1}{\gamma}\frac{(V_0 - V_{acc})^{\gamma+1}}{p_0 {V_0}^{\gamma}}\frac{\partial p_{acc}}{\partial t}, \tag{3.14}$$

Therefore, Equation (3.11) can be rewritten as:

$$q_{V\,acc} = \left(\frac{1}{\gamma}\frac{(V_0 - V_{acc})^{\gamma+1}}{p_0 {V_0}^{\gamma}} + \frac{V_{acc}}{\beta}\right)\frac{\partial p_{acc}}{\partial t}. \tag{3.15}$$

The accumulator flow rate can be determined by the corrected Bernoulli equation, incorporating the discharge coefficient c_d, where A_{acc} [m²] is the accumulator area. This is represented in Equation (3.16).

$$q_{V\,acc} = c_d A_{acc}\sqrt{\frac{2}{\rho}(p_S - p_{acc})}. \tag{3.16}$$

3.5. MODEL OF THE HYDRAULIC PUMP

In aircraft, the engine-driven pump (EDP) supplies pressurized hydraulic fluid to operate flight control surfaces and utility systems, making it the most critical component of the hydraulic system. A common EDP is a pressure compensated, variable displacement axial piston pump designed to deliver a variable volume of fluid to maintain consistent pressure in the hydraulic system (WANG *et al*., 2016).

According to Zhang *et al.* (2021), the axial piston pump is well-suited to the development and application of airborne hydraulic power sources, which demand a high power-to-weight ratio. Its compact structure, ability to operate at high pressures and speeds, and capacity for large flow rates make it widely used in aircraft hydraulic systems.

Ouyang (2016) points out that industrial piston pumps generally operate at rated speeds around 1500 rpm, while conventional aviation piston pumps function at much higher speeds, often exceeding 3000 rpm. For example, high-speed aviation pumps supplied by Parker Hannifin for Airbus and Boeing exceed 3500 rpm, with certain piston pumps reaching up to 22,500 rpm. However, achieving such high rotational speeds presents significant design and operational challenges, including cavitation, flow and pressure pulsation, and increased noise. These issues can reduce volumetric and mechanical efficiency and, in extreme cases, lead to pump failure.

As observed by Kollek *et al.* (2007), cavitation occurs during the oil suction stage when the piston is pulled out of the cavity, creating a void that needs to be filled with oil. However, at high speeds, the pump's inlet pressure may not be sufficient to compensate for throttling and flow losses, preventing the piston cavity from filling properly, which leads to cavitation.

An approach to deal with cavitation is to incorporate a bootstrap reservoir into the aircraft's primary hydraulic system. When the pump operates, high-pressure oil flows into the bootstrap chamber, generating boost pressure that moves the reservoir piston into the reservoir chamber. This movement pressurizes the reservoir chamber, ensuring a constant pressure is maintained. The piston continuously reciprocates to sustain the necessary inlet pressure for the hydraulic pump (OUYANG *et al*., 2018; YANG *et al*., 2012).

The operational principle of the piston pump is shown in Figure 3.8.

Figure 3.8 - Operational principle of a piston pump.

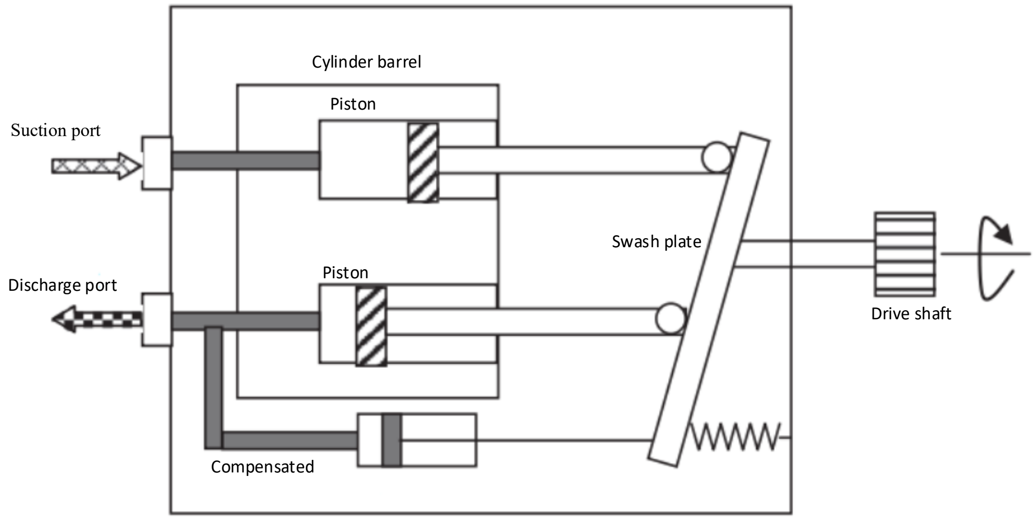

Source: Adapted from (WANG et al., 2016).

3.5.1. Continuity equation applied to the pump

The Figure 3.9 shows the scheme of an axial piston pump and its principal components.

Figure 3.9 - Schematic drawing for axial piston pump.

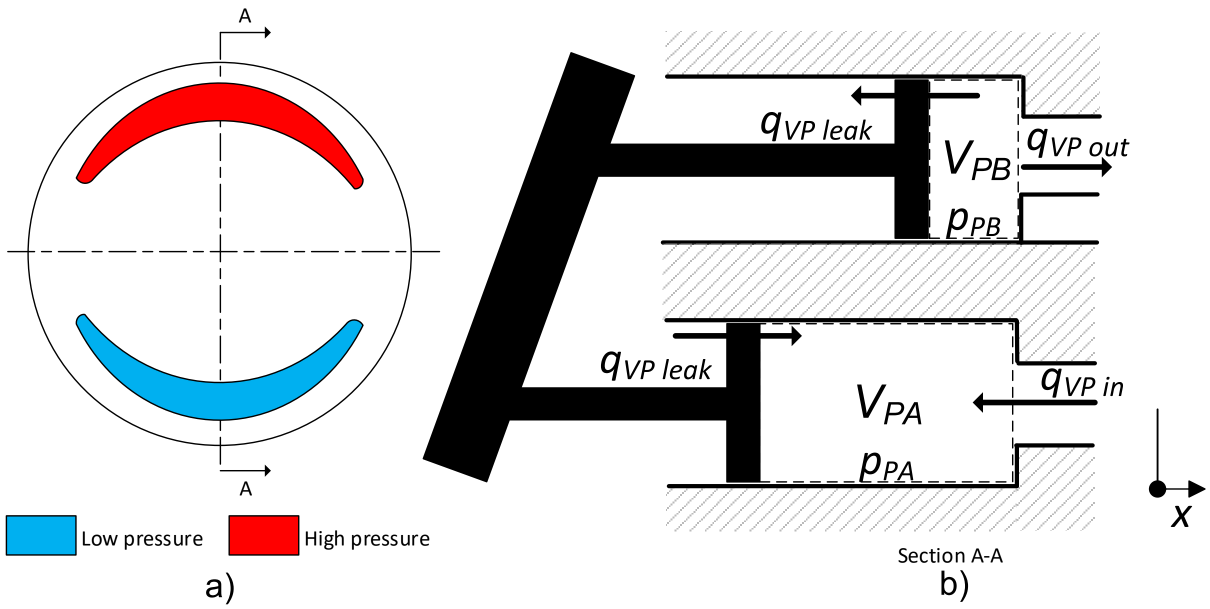

Source: By the author.

According to Figure 3.9 and applying the continuity equation on the A and B chambers of the hydraulic axial piston pump yields equations (3.17) and (3.18), respectively as follows

$$q_{VP\ in} + q_{VP\ leak} = D\omega + \frac{V_{PA}}{\beta}\frac{\partial p_{PA}}{\partial t}, \tag{3.17}$$

$$-q_{VP\ out} - q_{VP\ leak} = -D\omega + \frac{V_{PB}}{\beta}\frac{\partial p_{PB}}{\partial t}, \tag{3.18}$$

where V_{PA} and V_{PB} [m³] are the volumes of chambers A and B, respectively, $q_{VP\ in}$, $q_{VP\ out}$ and $q_{VP\ leak}$ [m³/s] the flow rates in, out and leakage of the pump, respectively, D [m³/rev] is the pump displacement and ω [rev] is the pumps rotation.

The volume change of these chambers is calculated with Equations (3.19) and (3.20). The dead volume of the pump chamber is calculated with Equation (3.21).

$$V_{PA} = V_{P0}(1 + 0.95 sin\ \omega t), \tag{3.19}$$

$$V_{PB} = V_{P0}(1 - 0.95 sin\ \omega t), \tag{3.20}$$

$$V_{P0} = 2D\pi, \tag{3.21}$$

where V_{P0} [m³] are the dead volume of piston pump.

3.5.2. Pump flow rate

The hydraulic power transferred to the fluid is reduced compared to the mechanical power input due to various factors contributing to losses. These losses originate from internal and external leakages, pump cavitation, incomplete filling of the pump, fluid compressibility, and friction. The extent of these leakages is influenced by the differential pressure across the pump and the viscosity of the fluid, with the latter being directly influenced by the oil temperature (MANRING, 2005). For this reason, the pump volumetric leakage flow rate is estimated with Equation (3.22).

$$q_{VP\ leak} = K_{P\ leak}(p_S - p_T). \tag{3.22}$$

To determine the $K_{P\ leak}$ [m³/(sPa$^{0.5}$)] coefficient, catalog data of the pump was used. The catalog specifies the maximum flow rate at a given rotation and pressure differential. This coefficient can be calculated with Equation (3.23), with Δp being the pressure differential given in the catalog

$$K_{P\ leak} = \frac{q_{VP\ leak}}{\Delta p}. \tag{3.23}$$

3.6. MODEL OF RELIEF VALVE

Relief valves are installed between high-pressure and return low-pressure lines to regulate the maximum operating pressure in the high-pressure circuit. The primary components of the relief valve include a spring-loaded poppet. The representation for this valve is observed in Figure 3.10. The relief valve's opening pressure is directly controlled by the pre-compression of its spring, a crucial parameter in hydraulic system design (RABIE, 2009). This setting ensures optimal protection against overpressure scenarios, maintaining system integrity and functionality.

Figure 3.10 - Schematic drawing for the relief valve.

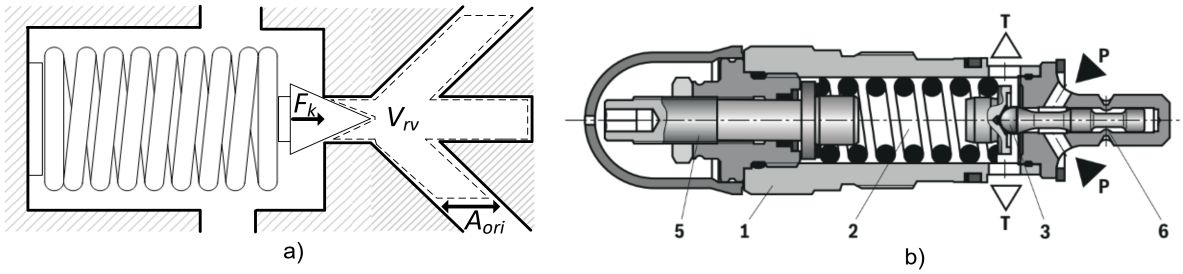

Source: a) By the author based on Rabie (2009); Adapted from Bosch Rexroth (2024).

Various safeguards are incorporated within hydraulic systems to mitigate the risk of overpressure. For instance, these safeguards play a critical role in preventing damage to high-pressure lines in the event of a malfunction in pump displacement adjustment (MARÉ, 2016).

3.6.1. Continuity equation applied on the relief valve

Applying the continuity equation for the control volume inside the valve yields Equation (3.24).

$$q_{Vrv\,in} - q_{Vrv\,out} = \frac{\partial V_{rv}}{\partial t} + \frac{V_{rv}}{\beta}\frac{\partial p_{rv}}{\partial t}. \tag{3.24}$$

Considering that there is no change in the volume of the relief valve ($\frac{\partial V_{rv}}{\partial t} = 0$), results in Equation (3.25).

$$q_{Vrv\,in} - q_{Vrv\,out} = \frac{V_{rv}}{\beta}\frac{\partial p_{rv}}{\partial t}, \tag{3.25}$$

where p_{rv} [Pa] is the pressure of the relief valve, $q_{Vrv\,in}$ and $q_{Vrv\,out}$ [m^3/s] the flow rates in and out of the relief valve, respectively, V_{rv} [m^3] is the volume of the relief valve.

3.6.2. Equation of motion applied to the relief valve

The dynamics of the relief valve can be obtained through Newton’s second law, in the Equation (3.26).

$$p_{rv}A_p - k(x_{rv} + x_0) - B\dot{x}_{rv} = M_{poppet}\ddot{x}_{rv}, \tag{3.26}$$

where k [N/m] is the stiffness of the spring, M_{poppet} [kg] is the mass of the relief valve spool, x_0 [m] is the pre-compressed length of the spring, x_{rv} [m] is the relief valve displacement and A_p [m²] is the valve area subjected to the pressure force.

According to Rabie (2009), the valve opening area can change nonlinearly with the displacement of the relief valve. For the modeling, a direct acting poppet-type pressure relief valves with a conical poppet will be used. The schematic for the valve opening area can be seen in Figure 3.11.

Figure 3.11 - Poppet relief valve area geometry.

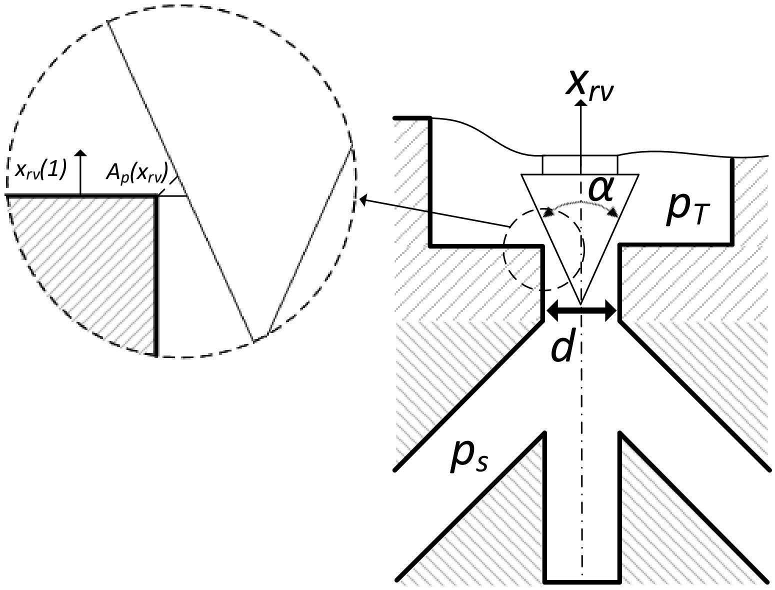

Source: By the author based on Lei *et. al.* (2017).

In comparison to spool valves, poppet valves offer several advantages. They exhibit no leakage when closed, eliminate the need for precise machining, and can adapt to wear over time. Additionally, poppet valves are insensitive to contamination particles, thanks to their self-flushing capability (MANRING, 2005).

When the poppet is in the position x_{rv} (1), shown as in Figure 3.11, the valve area subjected to pressure force A_p can be given as denoted in Equation (3.27) (RABIE, 2009).

$$A_p = \frac{\pi}{4}(d - 2x_{rv}sin\left(\frac{\alpha}{2}\right)cos\ \left(\frac{\alpha}{2}\right))^2, \tag{3.27}$$

where d [m] is the valve seat diameter and α [rad] is the cone vertex angle.

3.6.3. Equation of orifice for relief valve

In many cases, the fluid flow through an orifice is approximated to be proportional to the square root of the pressure drop across the orifice. This relationship is valid for steady-state, incompressible flow conditions and provides a reliable description, particularly for turbulent flow scenarios (BORUTZKY *et al.*, 2002). The flow that enters the relief valve can be calculated with Equation (3.28).

$$q_{Vrv\ in} = c_d A_{ori} \sqrt{\frac{2}{\rho}(p_S - p_{rv})}, \tag{3.28}$$

where A_{ori} [m²] is the orifice area of inlet for the pressure relief valve.

According to Rabie (2009), if the poppet is displaced by a distance x_{rv} (2), fluid is allowed to flow through the resulting open area. This open area consists of the lateral surface area of the truncated cone (abce). This resulting area can be observed in Figure 3.12.

Figure 3.12 - Conical poppet resulting flow through area.

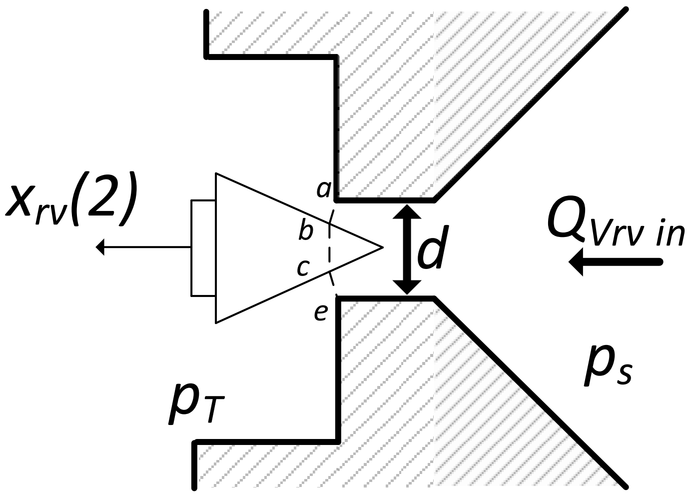

Source: By the author based on Rabie (2009).

The area A_t is calculated with Equation (3.29).

$$A_t = \pi x_{rv} sin\left(\frac{\alpha}{2}\right)\left\{d - x_{rv} sin\left(\frac{\alpha}{2}\right) cos\left(\frac{\alpha}{2}\right)\right\}. \tag{3.29}$$

Then, flow rate out of the relief valve can be calculated from Equation (3.30).

$$q_{Vrv\ out} = c_d A_t \sqrt{\frac{2}{\rho}(p_{rv} - p_T)}. \tag{3.30}$$

3.7. MODEL OF BOOTSTRAP RESERVOIR

According to Parker Hannifin Corporation (2023), bootstrap reservoirs store and deliver hydraulic fluid through a pressure-activated outlet, reducing air exposure to prevent cavitation and ensure consistent fluid supply. This compact design integrates easily into military and commercial hydraulic systems, as shown in the schematic Figure 3.13.

Figure 3.13 - Schematic representation for the bootstrap reservoir.

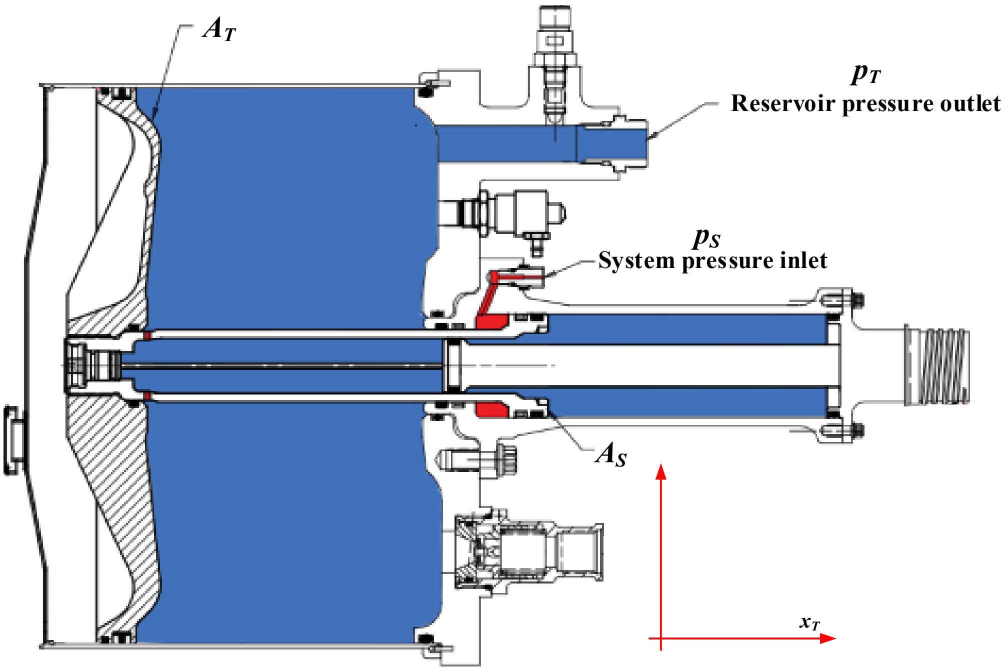

Source: By the author based on (PARKER HANNIFIN CORPORATION, 2023).

3.7.1. Continuity equation of the system pressure

Applying the continuity equation for the system side yields Equation (3.31). The system chamber volume can be calculated with Equation (3.32), and the change in volume with Equation (3.33).

System continuity equation:

$$q_{VP\,out} - q_{V\,acc} - q_{Vrv\,in} - q_{Vv\,in} - q_{vin\,pilot} = \frac{\partial V_S}{\partial t} + \frac{V_S}{\beta}\frac{\partial p_S}{\partial t}. \tag{3.31}$$

Volume change:

$$V_S = V_p + V_{S0} + A_S x_R, \tag{3.32}$$

$$\frac{\partial V_S}{\partial t} = A_S \dot{x}_R, \tag{3.33}$$

where V_S, V_{S0} and V_p [m³] are the reservoir system volume, system dead volume and piping volume, respectively, and A_S [m²] is the chamber area of the system actuator.

3.7.2. Continuity equation of the pressurized reservoir

For the reservoir, the continuity equation is represented by Equation (3.34). The reservoir chamber volume can be calculated with Equation (3.35), and the change in volume with Equation (3.36).

Reservoir continuity equation:

$$q_{Vrv\,out} + q_{Vv\,out} + q_{vin\,pilot} - q_{VP\,in} = \frac{\partial V_T}{\partial t} + \frac{V_T}{\beta}\frac{\partial p_T}{\partial t}. \tag{3.34}$$

Volume change:

$$V_T = V_p + V_{T0} + A_T x_R, \tag{3.35}$$

$$\frac{\partial V_T}{\partial t} = -A_T \dot{x}_R, \tag{3.36}$$

where V_T and V_{T0} [m³] are the pressurized reservoir volume and pressurized reservoir initial volume, respectively, A_T [m²] is the chamber area of the reservoir actuator.

3.7.3. Equation of motion applied to the bootstrap reservoir

The dynamics of the bootstrap reservoir can be determined using Newton's second law, as shown in Equation (3.37). This equation allows to calculate the displacement of the bootstrap reservoir.

$$p_S A_S - p_T A_T - B\dot{x}_R = M_T \ddot{x}_T, \tag{3.37}$$

where M_T [kg] is the total moving mass of the reservoir.

3.7.4. Force transmission and pressure differential in the bootstrap reservoir

From Figure 3.13, it can be observed that the two actuators are connected by the same rod. Since the rod is shared, the force exerted on both cylinders is identical. However, because the chamber areas differ, this constant force results in a pressure differential between the chambers. The magnitude of this pressure difference is directly proportional to the ratio of their respective areas, as demonstrated by Equation (3.38).

$$p_T = p_S \frac{A_S}{A_T}. \tag{3.38}$$

Since the area of the reservoir actuator is larger than the area of the system actuator, the pressure in the reservoir ends up being lower than the pressure in the system.

For instance, with a supply pressure is set at 7 MPa (70 bar) and an area ratio A_{ratio} (A_S/A_T) is set to 0.04, the reservoir pressure is approximately 0,28 MPa (2,8 bar).

This value is an approximation, as actual reservoir pressure can be slightly higher than calculated due to factors like system dynamics, fluid expansion, and minor leakage. These elements contribute to variations that maintain stability and efficiency in real-world operation.

While differences exist between the calculated static reservoir pressure and actual operating reservoir pressure, the estimated value still provides a useful basis for sizing the bootstrap reservoir. With a known supply pressure and the maximum allowable pump inlet pressure, this approximation guides reservoir design and helps ensure that the system meets operational pressure requirements.

4. PARAMETRIZATION OF COMPONENTS FOR SIMULATION

4.1. SIZING HYDRAULIC COMPONENTS

Furst & De Negri (2002) introduced a design procedure for sizing hydraulic positioning systems components, providing designers with control over technical decisions when developing electro-hydraulic positioners. This process is divided into three stages: (1) system and actuator characterization, (2) valve characterization, and (3) dynamic modeling and simulation. This methodology was further studied on Szpak (2008), Muraro (2009) and Destro (2014).

The first stage focuses on the system static and dynamic requirements, such as maximum displacement, response time, and maximum force. Mathematical expressions derived from the reference positioning model are used to determine the necessary specifications for both the valve and the cylinder. Since these components are interdependent, they must be sized simultaneously (DE NEGRI *et al.*, 2008).

For a hydraulic positioning system with a steady-state displacement x_{st} of 50 mm and a settling time t_s 1 s, the natural frequency of the system, for a second order dynamic behavior, can be expressed as (MURARO, 2009)

$$\omega_n = \frac{6}{t_s}, \tag{4.1}$$

which results in 6 rad/s. The maximum positive velocity can be evaluated as

$$v_{a\,maxp} = 0.37 x_{st} \omega_n, \tag{4.2}$$

resulting in 0.111 m/s.

The system consists of a symmetrical actuator and a symmetrical valve. Given this configuration and a supply pressure of 7 MPa (70 bar), the load pressure can be calculated as follows

$$p_L = \frac{2}{3} p_S, \tag{4.3}$$

resulting in 4.67 MPa (46.7 bar).

4.2. ACTUATOR CHARACTERIZATION

The actuator area, taking into account the load pressure, maximum velocity, and a load force F_L 6880 N, along with a viscous friction coefficient B of 1000 Ns/m, can be determined as follows

$$A_e = \frac{Bv_{a\,maxp} + F_L}{p_L}, \tag{4.4}$$

resulting in 1.5×10^{-3} m^2.

The load force of 6880 N was derived from the force generated by a symmetric double-acting pneumatic cylinder, the Festo-DGN-125-160-PPV-A-S2. This cylinder, which was also utilized in the study by Locateli (2011), features a 160 mm stroke, a piston diameter of 125 mm, and a rod diameter of 32 mm, resulting in an operational air area of 1.15×10^{-2} m^2. With a working pressure range from 0.6 to 10 bar and an operational temperature range of -20°C to 80°C, the selected pressure for this application was set at 6 bar. Using the pressure equation $(p = F/A)$, the calculated force was 6880 N. Further details about the actuator can be found in FESTO (2010). This cylinder was chosen because it is available at LASHIP for use in an experimental test bench, simulating the external load in the system.

The selected actuator is the Bosch Rexroth CGT3 MS2 50/22-500/Z1X/B1, which was also referenced in Silva Neto (2021). This actuator is symmetric, with equal areas in both chambers. The selection criteria require that the actuator's area must be larger than the calculated minimum. In this case, the actuator area is 1.58×10^{-3} m^2. which is larger than the calculated requirement 1.5×10^{-3} m^2. General specifications for this actuator are provided in the Bosch Rexroth catalog (2024b) and summarized in Table 4.1.

Table 4.1 - Parameters for the hydraulic actuator.

Parameter	Description
Model type	CGT3 MS2 50/22- 500
Cylinder Ø	0.05 m
Cylinder rod Ø	0.022 m
Cylinder stroke	0.5 m
Cylinder area	1.58×10^{-3} m²
Cylinder volume	3.95×10^{-4} m³
Total mass	13.1 kg

Source: Adapted from Bosch Rexroth (2024b).

4.3. PUMP CHARACTERIZATION

The total supply flow rate can be computed as

$$q_{VP\ in} = A_A v_{a\ maxp}, \tag{4.5}$$

which results in 1.76×10^{-4} m^3/s (10.55 L/min).

The selected piston pump is the Bosch Rexroth AV10VO series 53. The general specifications for this pump are listed in the Bosch Rexroth catalog (2024c) and are summarized in Table 4.2.

Table 4.2 - Parameters for the hydraulic axial piston pump.

Parameter	**Description**
Pump type code	A10VO Series 53
Maximum flow rate	59 L/min
Volumetric displacement	18 cm³
Suction port area	7.9×10^{-4} m²
Outlet port area	2.8×10^{-4} m²
Piston chamber volume	6×10^{-5} m³

Source: Adapted from Bosch Rexroth (2024c).

To meet the required flow rate, the pump rotation was set to 1500 rpm, and the volumetric displacement was adjusted to 9.5 cm³. This configuration resulted in a flow rate of 14.25 L/min, which is 35% higher than the required value to account for leakages in the system components, such as servo-valve, actuator.

4.4. VALVE CHARACTERIZATION

Solving Equation (4.4) for load pressure $p_{L\ vmax}$, formulated as following

$$p_{L\ vmax} = \frac{B v_{a\ maxp} + F_L}{A_A}, \tag{4.6}$$

results in 4.42 MPa (44.2 bar).

Using the maximum load pressure calculated, the total pressure difference across the valve can be estimated, considering a symmetrical valve as:

$$\Delta p_T = p_S - p_{L\ vmax}, \tag{4.7}$$

resulting in 2.58 MPa (25.8 bar).

Thus, the flow coefficient can be assessed as

$$K_v = \frac{q_{VP\ in}}{\sqrt{\Delta p_T}}, \tag{4.8}$$

resulting in 1.1×10^{-7} m^3/(sPa$^{0.5}$).

The verification criteria are outlined in Equation (4.9). According to this equation, the flow coefficient from the catalog must not exceed twice the calculated flow coefficient, nor be less than half of the calculated value.

$$\frac{K_v}{2} \leq K_{v\,cat} \leq 2K_v, \tag{4.9}$$

The Moog manufacturer catalog (2007) provides information for each size of the servo valve, from which the total flow coefficients (K_v) for each size was calculated in Table 4.3.

Table 4.3 - Flow coefficients of servo valve (K_v).

Nominal flow rate Δp = 7 MPa (70 bar)		**Kv**
gpm	**m³/s**	**m³/(s√Pa)**
1	6.31×10^{-5}	2.40×10^{-8}
2,5	1.58×10^{-4}	6.01×10^{-8}
5	3.15×10^{-4}	$1.20 \text{ x } 10^{-7}$
10	$\mathbf{6.31 \times 10^{-4}}$	$\mathbf{2.40 \times 10^{-7}}$
15	9.46×10^{-4}	3.61×10^{-7}

Source: Adapted from MOOG (2024).

The selected nominal size for the valve should be 5 gpm to meet the verification criteria. However, the 10 gpm valve was selected instead because it is available at LASHIP. Although this valve does not fully meet the criteria from Equation (4.9), its dynamic performance will be evaluated to determine if the discrepancy poses any issues on simulation results.

Table 4.4 presents more information about the selected MOOG servo valve and parameters that are used in the simulation.

Table 4.4 - Parameters for the servo valve.

Parameter	**Description**
Model type	760C262A - 10 gpm
Configuration	4/3 ways, closed center
Nominal flow rate	6.31×10^{-4} m³/s @ 7 MPa
Total flow coefficient	2.40×10^{-7} @ 7 MPa
Spool diameter	6.6 mm
Radial clearance	min 2.54 µm - max 4.32 µm
Nominal voltage	10 V
Natural frequency	87.3 Hz
Damping ratio	0.9

Source: Adapted from MOOG (2024).

The total flow coefficient was determined based on the nominal flow rate. The natural frequency of the valve was identified from the frequency response curve by locating the -90 degree phase-lag point, which defines the valve's bandwidth. The frequency response curve is shown in Figure 4.1. The damping ratio was assumed to be a typical value of 0.9.

Figure 4.1 - Frequency response for MOOG 760C262A.

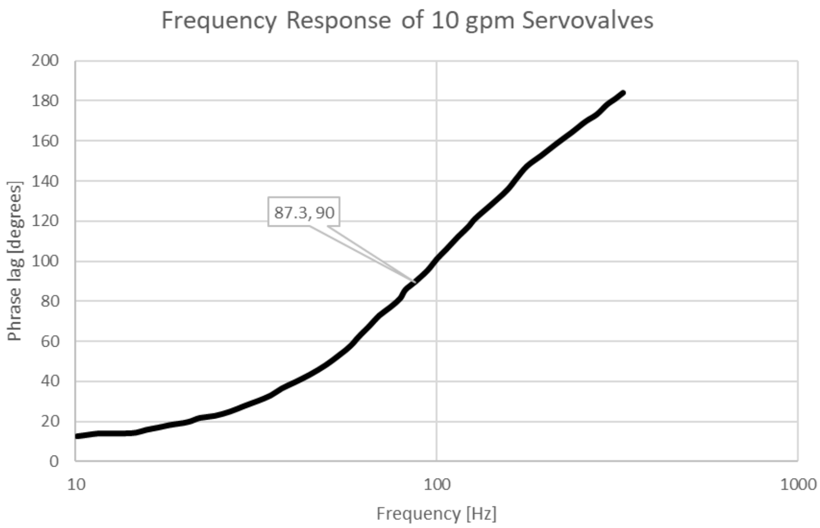

Source: By the author based on MOOG (2024).

In servo valves, there are two main sources of leakage: one originating from the clearance between the spool and the valve's sleeve, leading to radial internal leakage, and pilot leakage, that occurs because the pilot stage typically operates at a higher pressure to generate the necessary forces to move the main spool. To maintain system pressure, the variable displacement pump must compensate for this internal leakage. However, when the cylinder is not moving, the pump operates at very low displacement settings, which degrades volumetric efficiency of the pump (Pinto *et al.*, 2016; Maré, 2016). In this study, however, a fixed displacement pump model is used.

The parametrization for the radial internal leakage was based on the internal leakage curve obtained from experiments conducted by engineer Ivan Junior Mantovani. These experiments involved a Moog 760 C263-A servo valve, which has a nominal flow rate of 6.3 $\times 10^{-4}$ m³/s at 7 MPa (10 gpm), using the pneumatic positioner test bench and the IBYTÚ unit available at LASHIP (Laboratory of Hydraulic and Pneumatic Systems).

The experiments to generate the internal leakage curve for the servo valve were conducted in accordance with ISO 10770-1, section 8.1.3 - Internal Leakage Test (control ports blocked). During the experiment, the servo valve was supplied with an input voltage signal ranging from -3 to 3 V, with ports A and B closed. The flow from the supply line was measured using a sensor. Figure 4.2 presents the two curves obtained by engineer Mantovani, and also a model curve.

Figure 4.2 - Servo valves radial internal leakage.

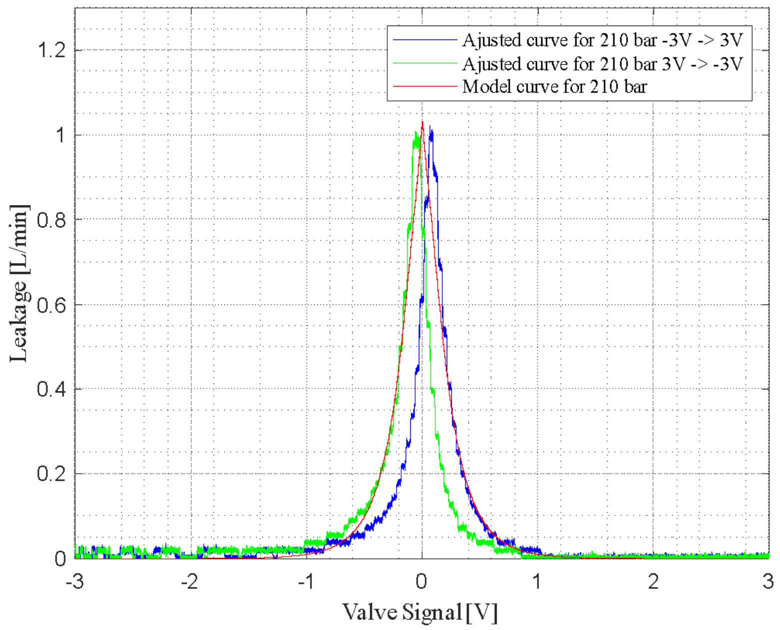

Source: By the author using the data provided by Ivan Mantovani and Cruz (2018).

The key parameter for specifying the servo valve radial internal leakage is the total leakage flow coefficient (K_{vin}). From Figure 4.3, the leakage flow coefficient can be determined by dividing the maximum leakage 1.67×10^{-5} m³/s (1 L/min) by the square root of the pressure, which is 21 MPa (210 bar). The resulting value for K_{vin} is 3.63×10^{-9} $\mathrm{m}^3/(\mathrm{s}\sqrt{\mathrm{Pa}})$.

The parameterization of the servo valve pilot leakage model was based on the internal leakage curve obtained from experiments conducted by engineer Ivan Junior Mantovani. Figure 4.3 presents the internal leakage curves with and without pilot operation, as well as the pilot flow curve.

Figure 4.3 - Internal leakage curve with and without pilot leakage of the servo valve.

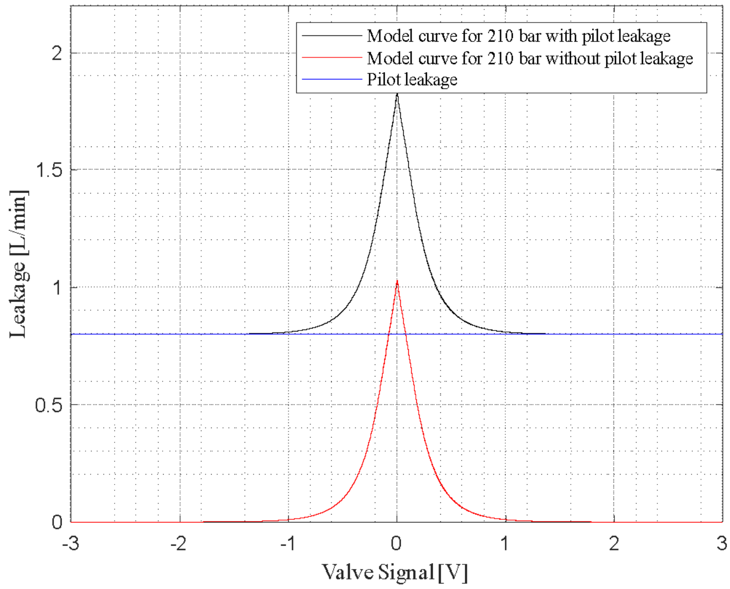

Source: By the author using the data provided by Ivan Mantovani and Cruz (2018).

The pilot leakage coefficient can be calculated by dividing the pilot leakage flow rate 1.33×10^{-5} m³/s (0.8 L/min) by the square root of the pressure differential by the square root of the pressure, which is 21 MPa (210 bar). The resulting value for $K_{vin\,pilot}$ is 2.90×10^{-9} $\mathrm{m^3/(s\sqrt{Pa})}$.

4.5. PRESSURE RELIEF VALVE CHARACTERIZATION

The relief valve parameters can be characterized by identifying parameters such as the orifice inlet area, the mass of the poppet, the valve's internal volume, the diameter of the circular seat, the cone's vertex angle, and the stiffness of the spring.

The chosen relief valve model is the Bosch Rexroth DBD-NG6-6-K-1X-315. The internal details and poppet can be observed in Figure 4.4. Its detailed specifications can be found in the Bosch Rexroth catalog (2024a) and are summarized in Table 4.5.

Figure 4.4 - Poppet seat relief valve.

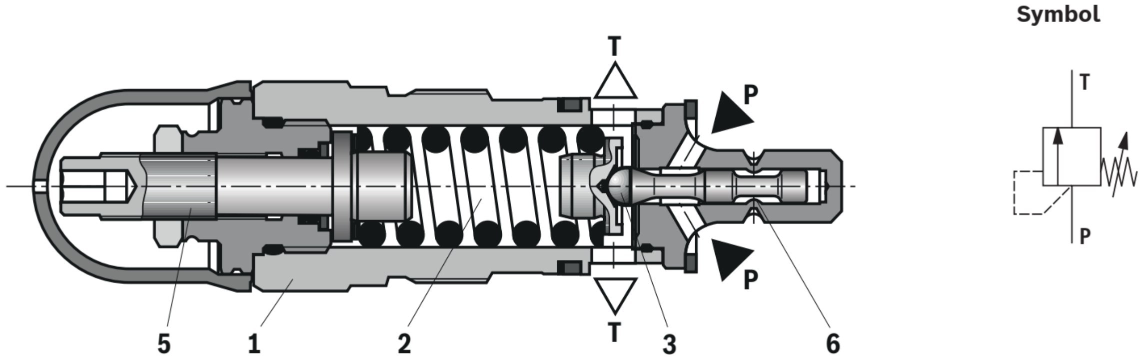

Source: Bosch Rexroth (2024a).

Table 4.5 - Parameters for the relief valve.

Parameter	Description
Model type	DBD-NG6-6-K-1X-315
Orifice inlet area	1.13×10^{-4} m²
Poppet mass	0.1 kg
Volume relief valve	1.63×10^{-6} m³
Diameter of the circular poppet seat	0.004 m
Cone vertex angle	60°
Spring stiffness	22000 N/m

Source: Adapted from Bosch Rexroth (2024a).

4.6. ACCUMULATOR CHARACTERIZATION

According to Vacca & Franzoni (2021) and Ledezma (2012), the pre-charge pressure should be between 70% and 90% of the working pressure. In any gas-charged accumulator, the precharge value is defined as the pressure in the gas chamber when the accumulator is fully empty of hydraulic fluid. The precharge can be adjusted by introducing or relieving gas through the valve at the gas inlet. Given a working pressure of 75 bar, a pre-charge pressure set at 90% would correspond to 67.5 bar.

The selected accumulator is the HYDAC metal bellows accumulator, model SM50P-0.38WE1/116U. The inlet for this accumulator consists of a cylinder opening with a diameter of 12.7 mm. Its general specifications are detailed in the HYDAC Technology GmbH catalog (2024) and summarized in Table 4.6.

Table 4.6 - Parameters for the accumulator.

Parameter	**Description**
Model type	SM50P-0.38WE1/116U
Precharge pressure	6.75×10^{6} Pa
Accumulator volume	3.8×10^{-4} m³
Accumulator inlet/outlet area	1.27×10^{-3} m²

Source: Adapted from HYDAC Technology GmbH (2024).

4.7. BOOTSTRAP RESERVOIR

The selected reservoir is the Parker Bootstrap Reservoir, part number 3810041, with a maximum reservoir pressure of 2.75 bar. It includes an integrated filter/reservoir module and a dirty filter indicator for real-time monitoring of filter condition. This feature ensures timely maintenance and minimizes the risk of contamination in the hydraulic system. Detailed specifications for the bootstrap reservoir can be found in the Parker Hannifin Corporation catalog (2023) and are summarized in Table 4.7.

To determine the supply actuator area, Equation (3.38) was used, as Parker's catalog provides only the reservoir actuator area.

Table 4.7 - Parameters for the bootstrap reservoir.

Parameter	**Description**
Model type	Parker 3810041
Low pressure cylinder area	4.8×10^{-2} m²
High pressure cylinder area	1.9×10^{-3} m²
Area ratio	0.04
Reservoir mass	19.2 kg

Source: Adapted from Parker Hannifin Corporation (2023).

5. SIMULATION AND RESULTS

5.1. INTRODUCTION

The analysis will involve two reference inputs. The first is a step input, used to verify the settling time (t_s 1 s), as discussed in Section 4.1. The second input comes from the right aileron of the hydraulic system configuration based on the military aircraft SAAB JAS 39 Gripen (KARLSSON, 1985), applied using the *F16systemManeuver* model in Hopsan software (KRUS *et al*., 2012). A similar study of the left aileron was conducted by Cruz (2018).

The simulations were conducted in MATLAB, a widely used computational tool for dynamic system analysis and control. For this study, the ode14x solver was selected, which utilizes an extrapolation method to compute the system states at each time step. The solver was configured with a fixed-step size of 1×10^{-4}, an extrapolation order of 4, and a single Newton's iteration per step.

Figure 5.1 displays the step reference input, while Figure 5.2 shows the right aileron profile.

Figure 5.1 - Step reference input.

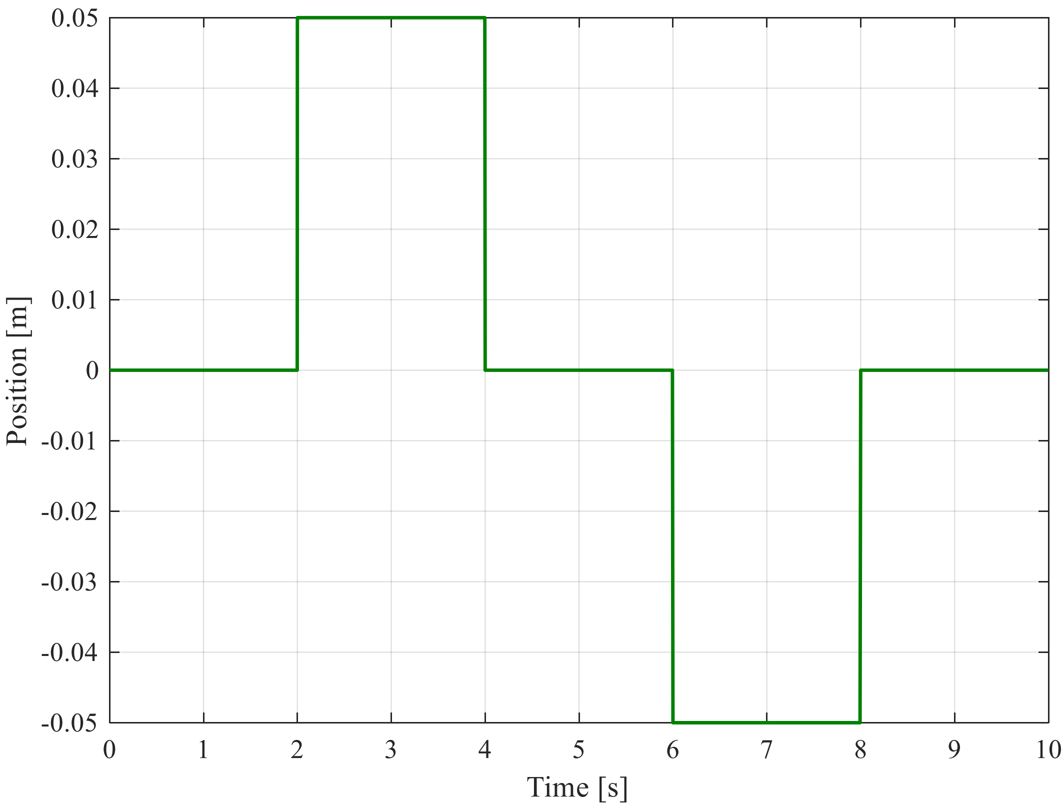

Source: By the author.

Figure 5.2 – Right aileron reference input.

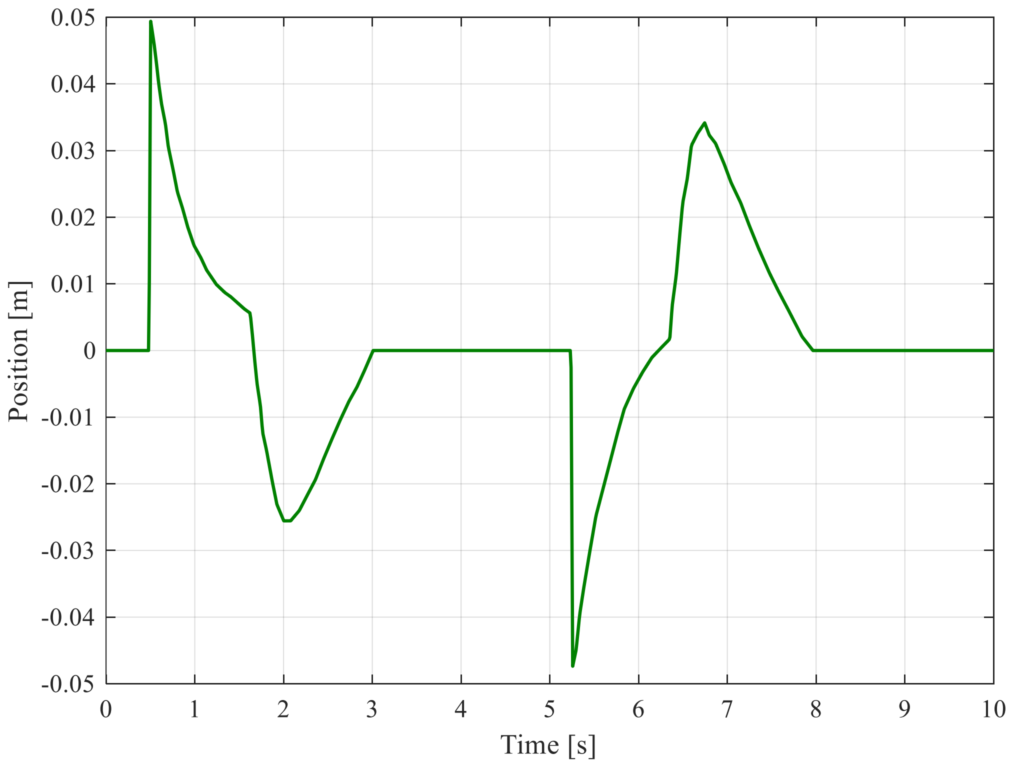

Source: By the author.

5.1.1. System control PI

In this section, the control strategy for the system in a closed-loop configuration is presented, with the schematic block diagram shown Figure 5.3.

Figure 5.3 - System control block diagram.

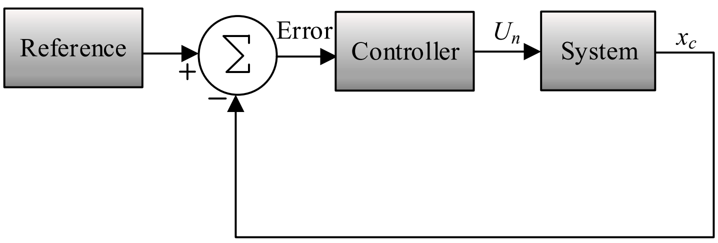

Source: By the author.

The system operates as follows: a reference signal is applied and compared to the actual position of the actuator, x_c, generating a position signal error. This error is then sent to the controller, which produces the control signal U_n. This signal serves as the input to the servo-valve, adjusting the system to achieve the desired reference position x_c.

A PI (Proportional-Integral) controller was chosen for this system due to its easy implementation and successful application in similar hydraulic systems. Many studies, including those by Szpak (2008), Belan *et al*. (2015), Silva Neto (2021), and Nostrani (2021), have demonstrated the effectiveness of PI or PID controllers in achieving accurate and stable performance in hydraulic positioning systems. The PI controller is presented in Figure 5.4.

Figure 5.4 - PI controller block diagram.

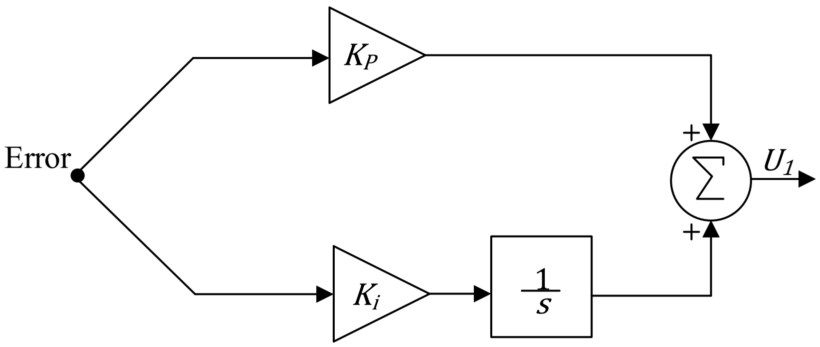

Source: By the author.

For this work, the selected proportional gain K_P (V/m) was set to 200. This value was determined based on the need to convert the maximum input step of x_{st} of 50 mm to an equivalent voltage of 10V for the servo-valve. The integral gain K_i V/(m.s) was adjusted during simulation tests and set to 0.1 aiming to eliminate steady-state error.

5.2. RESULTS FOR STEP REFERENCE

Figure 5.5 illustrates the response of the actuator. The reference signal is represented by the dashed green line, while the blue line indicates the actual position of the actuator. The system achieves an accommodation time t_s of 0.975 s, measured based on a 2% settling criterion as defined by Ogata (2010), which specifies the time for the response to remain within 2% of the final value. With a steady-state displacement x_{st} is 50 mm, the displacement value should reach 49 mm to measure the accommodation time of 0.975 s, as shown in Figure 5.5

The initial design calculations using Furst and De Negri's (2002) methodology set the accommodation time at 1 s, and the system achieved the desired response, reaching the target position within 0.975 s.

Figure 5.5 - Position response for position control with step reference.

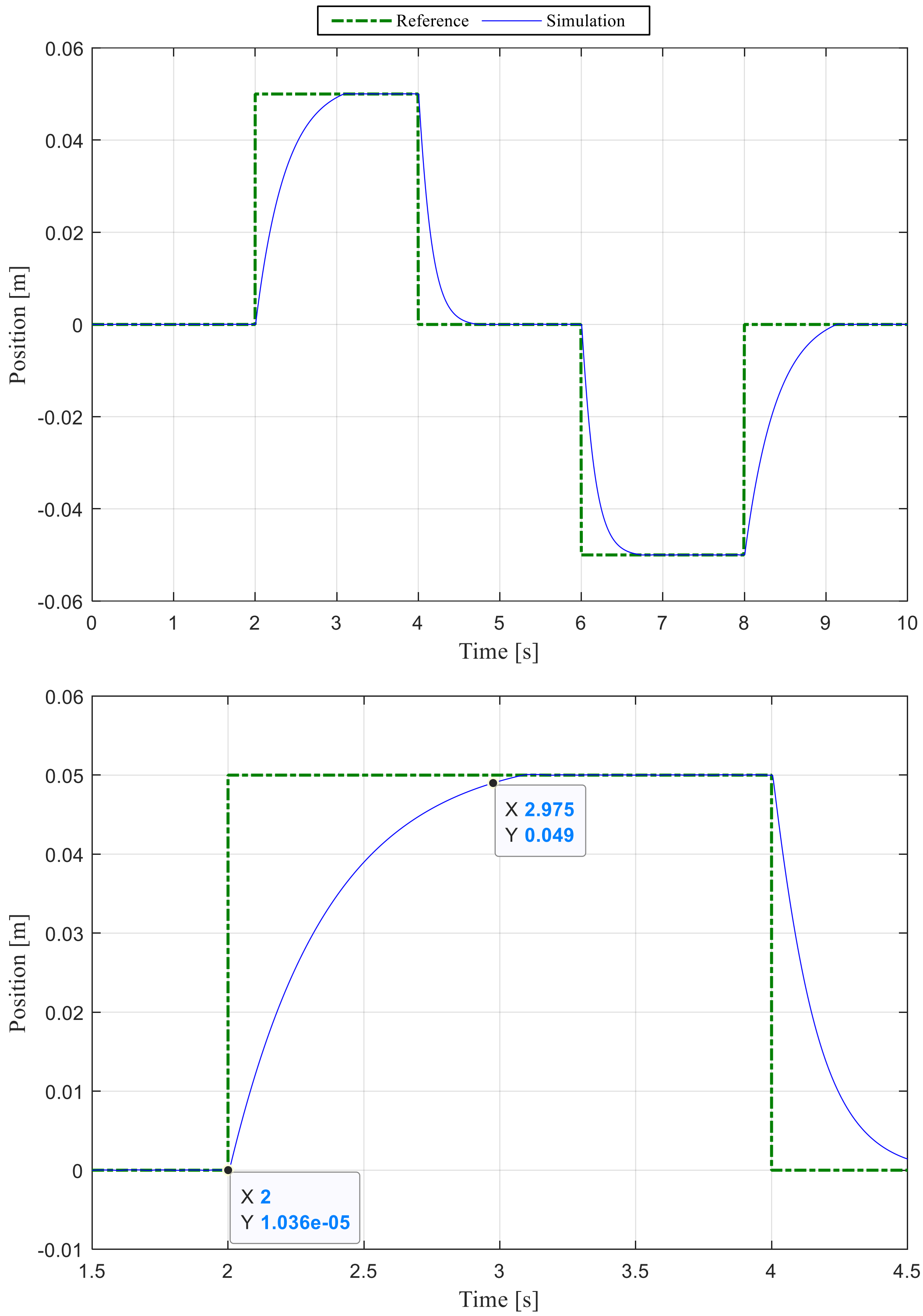

Source: By the author.

Figure 5.6 illustrates the behavior of both the system and reservoir pressures. As the actuator moves, the pressure fluctuates in response to the fluid entering and exiting the reservoir.

In Figure 5.6, although the external load remained constant and continued to act on the control surface, the reservoir pressure decreased by only 0.2 bar, maintaining sufficient suction pressure for the pump. This demonstrates an advantage of bootstrap reservoirs, which can stabilize reservoir pressure even under sustained loads.

According to calculations in Section 3.7.4, the reservoir pressure was calculated to be 2.8 bar based on a static analysis, while the dynamic system achieved a slightly higher pressure of 2.914 bar. This difference arises from the pressure ratio between chambers connected by a shared rod, where the force remains constant but the pressure varies due to differing chamber areas, as shown in Equation (3.38). With a system pressure of 73.9 bar and a bootstrap reservoir area ratio of 0.04, the resulting reservoir pressure dynamically reaches 2.914 bar, close to the calculated value yet accounting for factors that influence the dynamic model.

Figure 5.6 – System and reservoir pressures for position control with step reference.

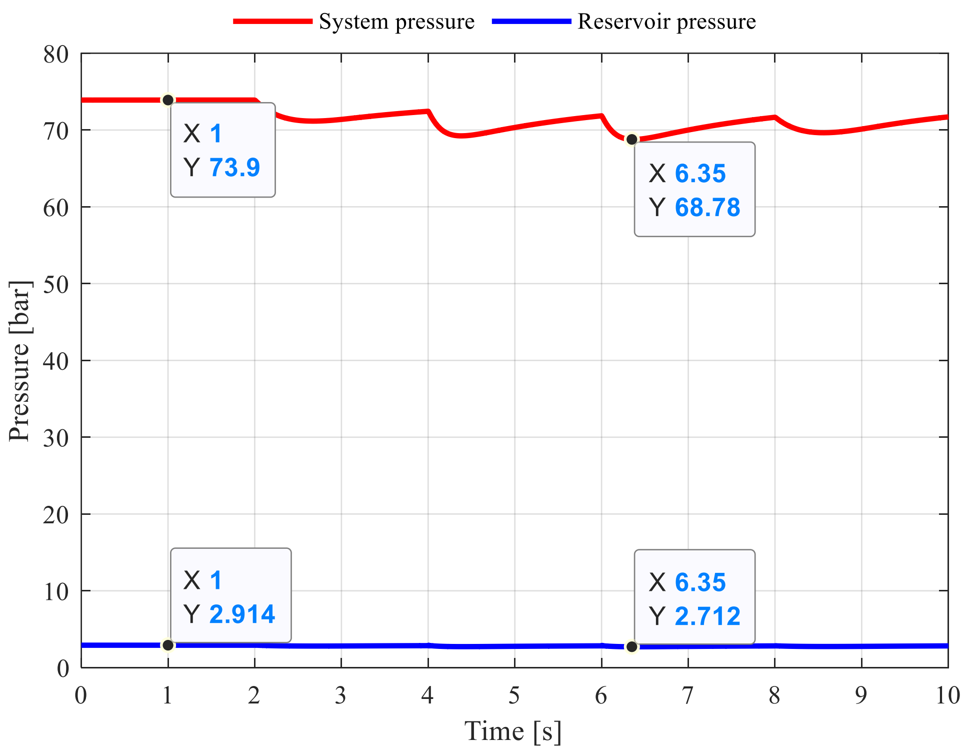

Source: By the author.

Figure 5.7 illustrates the actuator pressure dynamics. When a positive command signal U_n is issued, the servo-valve shifts to a parallel connection, leading to an increase in pressure within Chamber A and a corresponding decrease in Chamber B. In a hold or stop position, slight pressure fluctuations in both chambers are observed, indicating minor internal leakage within the servo-valve. This leakage is primarily due to radial clearance in the spool of the servo-valve and pilot leakage. When the actuator is commanded to retract, pressure in Chamber B increases while pressure in Chamber A decreases. To counteract the load force F_L 6880 N, a working pressure $(p_A - p_B)$ of approximately 40 bar is necessary, ensuring that the actuator can maintain its position against the applied load.

Some of the flow is diverted to compensate for internal and pilot leakage in the servo-valve. This leakage is evident in the pressure variations seen in Figure 5.7 for chambers A and B of the actuator.

Figure 5.7 - Cylinder chambers pressure for position control with step reference.

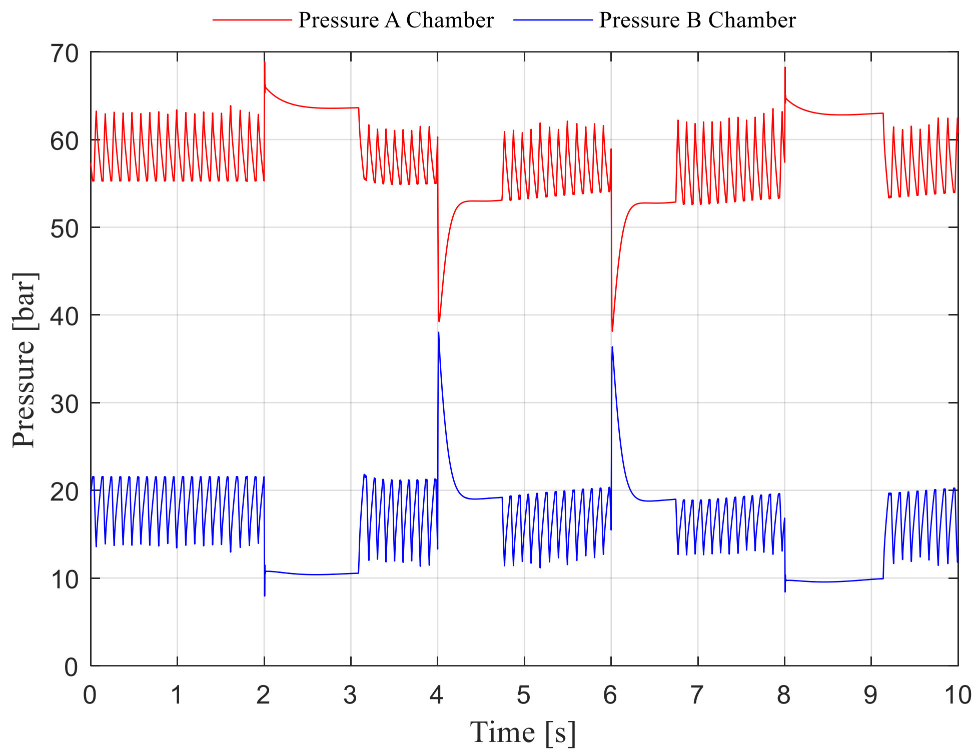

Source: By the author.

Figure 5.8 shows the command signal sent to the servo-valve. It confirms that the proportional gain, set to 200 on Section 5.1.1, correctly adjusts the control signal to 10V for a step input of 50 mm. Additionally, during the time interval from 0 s to 2 s, the controller attempts to follow the reference position of 0 mm. However, the significant leakage observed in Figure 4.3 – 0.5 L/min of pilot leakage and 0.8 L/min of internal leakage – results in the pressure variations shown in Figure 5.7 as the actuator works to maintain the reference position.

In Section 5.2.1 a lower leakage coefficient K_{vin} will be applied, and the resulting actuator pressure and command signal will be analyzed.

Figure 5.8 – Command signal for position control with step reference.

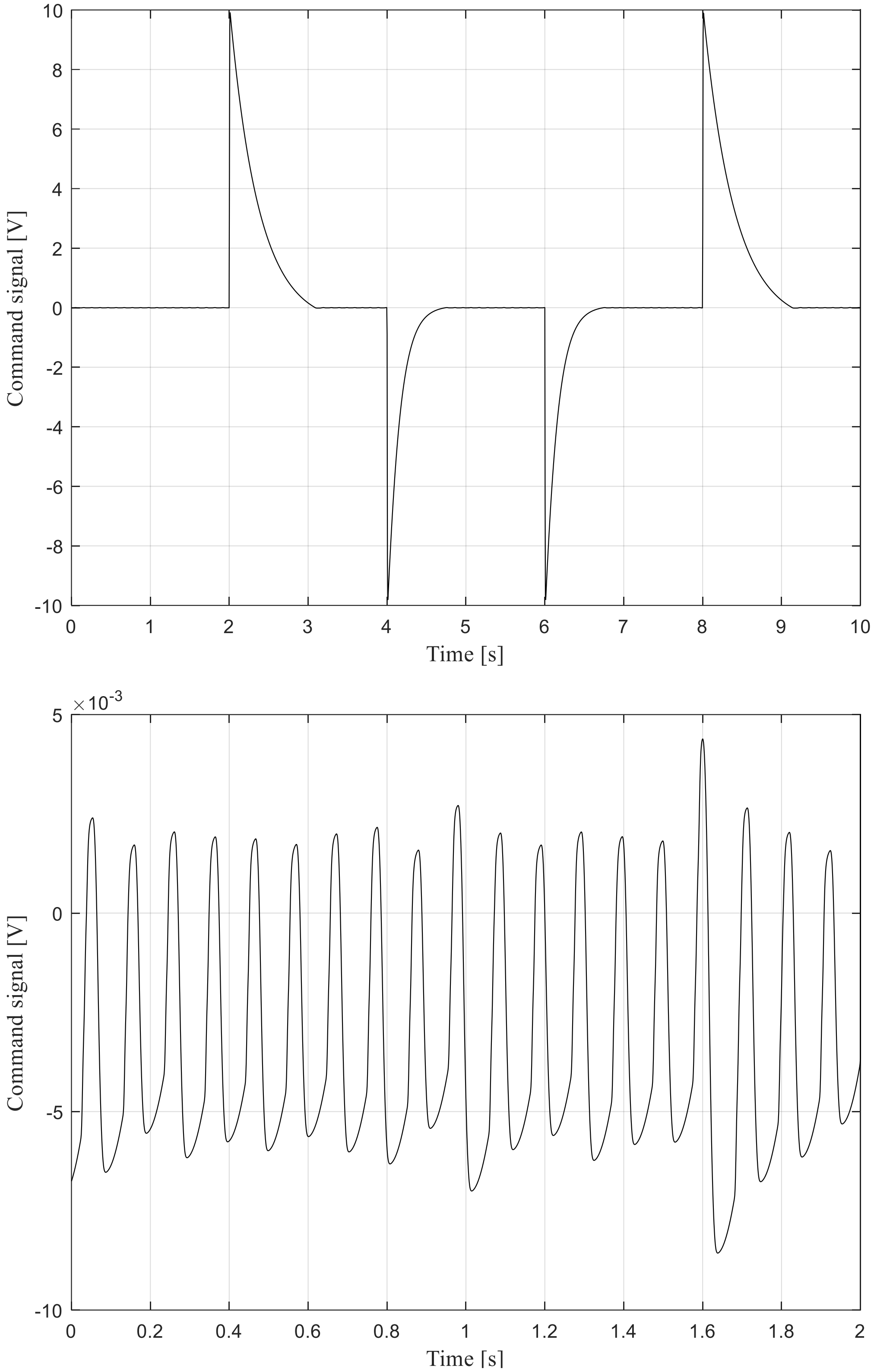

Source: By the author.

Figure 5.9 illustrates the reservoir position in response to the actuator's flow demands. When the actuator moves, there’s a higher flow requirement, which causes the reservoir position to decrease, indicating a reduction in its volume as fluid is supplied to the control surface. The reservoir reaches an equilibrium position of 1.795 mm.

During the first step input, the reservoir position decreases from 1.795 mm to 0.67 mm, indicating a reduction in volume as the reservoir provides the required flow to move the actuator. For the second step input, the reservoir position further drops from 0.67 mm to nearly 0 mm, leaving approximately half of its volume. Subsequent steps continue to drain the reservoir, supplying the flow needed for the actuator to reach the desired position.

In periods when the actuator is stationary—from 3 to 4 seconds, 5 to 6 seconds, 7 to 8 seconds, and 9 to 10 seconds—the reservoir refills, as indicated by the increase in reservoir position.

Figure 5.9 – Reservoir position for position control with step reference.

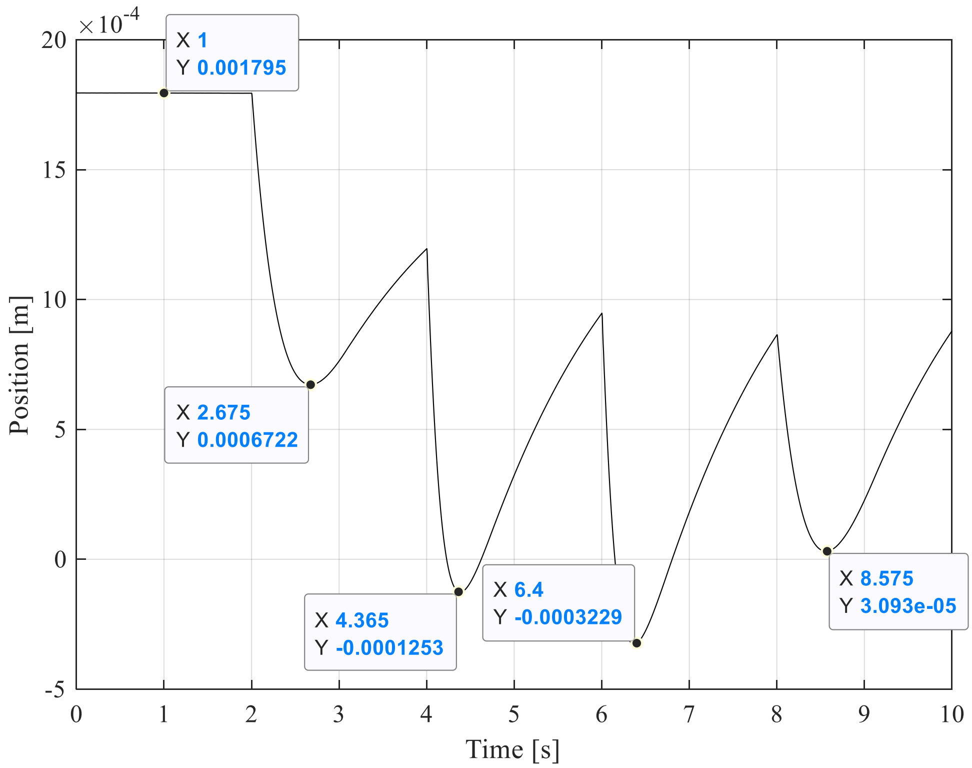

Source: By the author.

In Figure 5.10, the pump supplies a constant flow rate of 14.15 L/min to the system. When the actuator is in motion, this flow is directed through the servo valve. However, during intervals when the actuator is stationary, such as from 0 to 2 seconds, the pump continues running—as it is a fixed displacement pump—and the entire flow is diverted to the relief valve.

For actuator positioning during control surface movements, the accumulator provides additional flow to meet demand. After this, the pump replenishes the accumulator, restoring its volume for future flow requirements.

Figure 5.10 – Flow rates for position control with step reference.

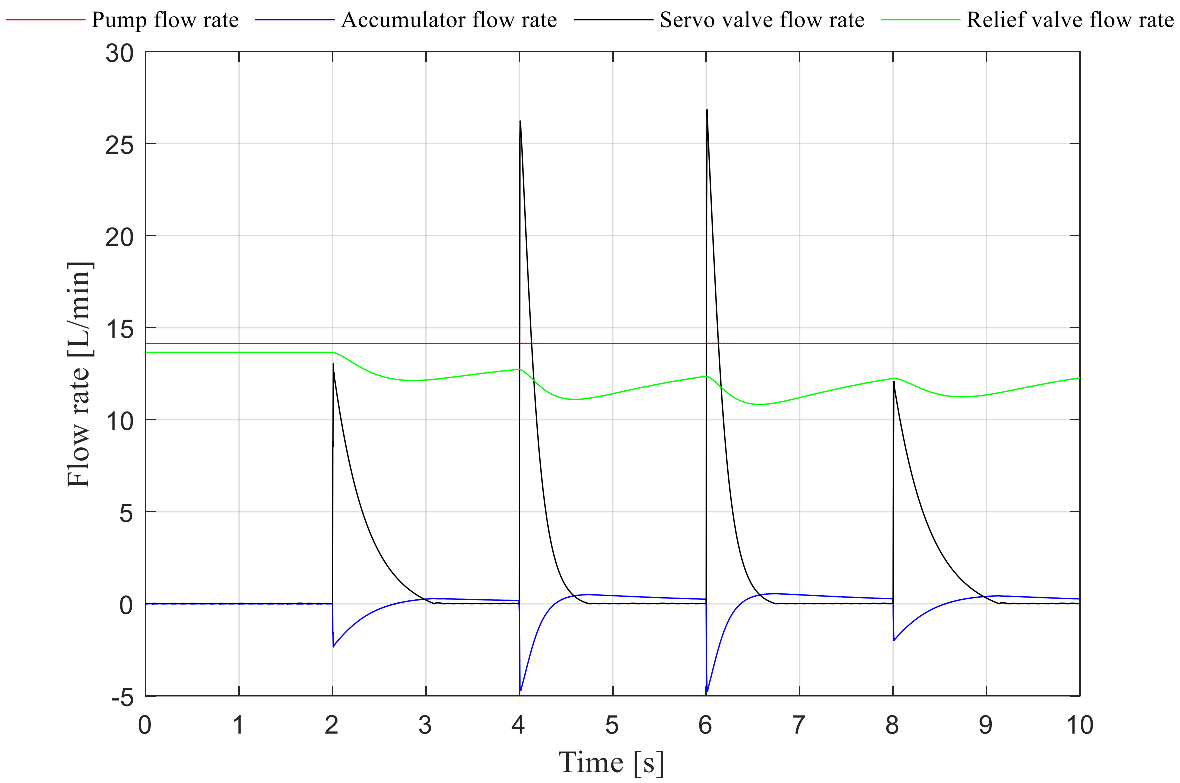

Source: By the author.

5.2.1. Internal leakage lowered by a power of 10

As shown in Figure 5.11, reducing the K_{in} by a power of 10 reduces the amplitude of pressure oscillations in the actuator chambers. These oscillations occur because the servo valve experiences both internal and pilot leakages, causing the actuator's position to fluctuate. The controller responds by adjusting the actuator position to match the reference.

Even reducing the integral gain or switching to a proportional controller alone does not resolve this issue in the no-displacement condition. This is due to the small overlap in the servo-valve spool, which results in a combined leakage flow rate of approximately 1 L/min. Consequently, the leakage causes continuous updates to the actuator position, creating flow in the small actuator chamber volume. This high flow rate, in turn, leads to the observed pressure oscillations.

In Figure 5.12, the command signal also decreases by an order of 10, compared to Figure 5.8.

Figure 5.11 – Cylinder chambers pressure for position control with step reference and lower leakage.

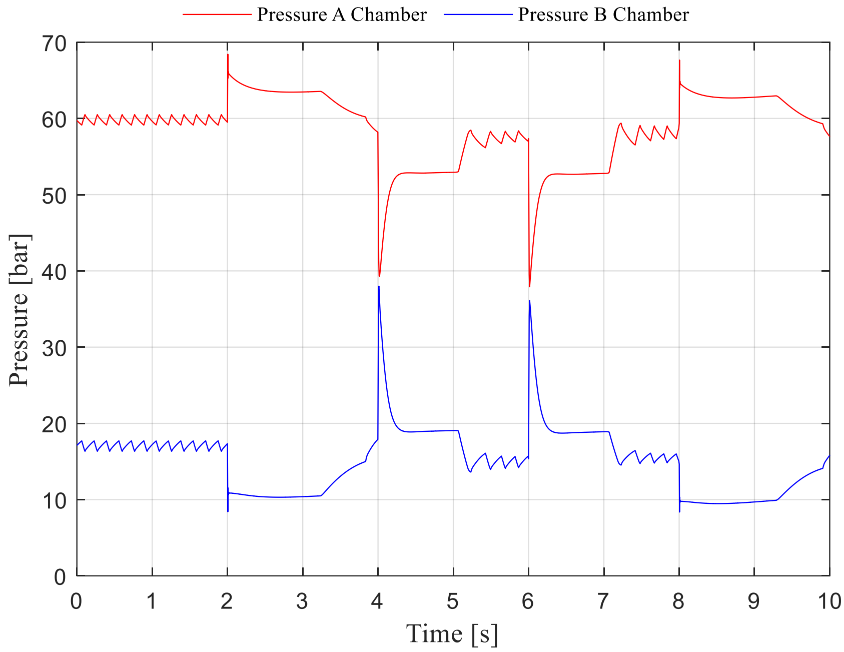

Source: By the author.

Figure 5.12 – Command signal for position control with step reference and lower leakage.

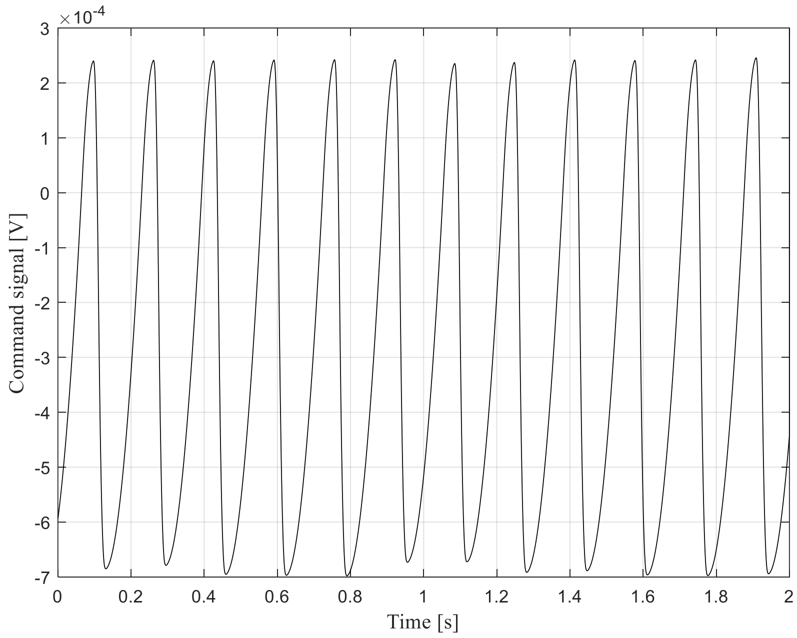

Source: By the author.

5.3. RESULTS FOR RIGHT AILERON REFERENCE

Figure 5.13 presents the actuator response under control of the right aileron surface. The system was designed for an accommodation time t_s of 1 second. However, as shown in Figure 5.13, the actuator struggles to follow the control input accurately. Notably, at approximately 0.5 seconds and 5.2 seconds, impulse position changes occur, and the actuator is too slow to respond effectively. Similarly, at 6.4 seconds, while the actuator follows a ramp input, the system can’t keep up with the reference trajectory.

Figure 5.13 – Position response for position control with aileron reference.

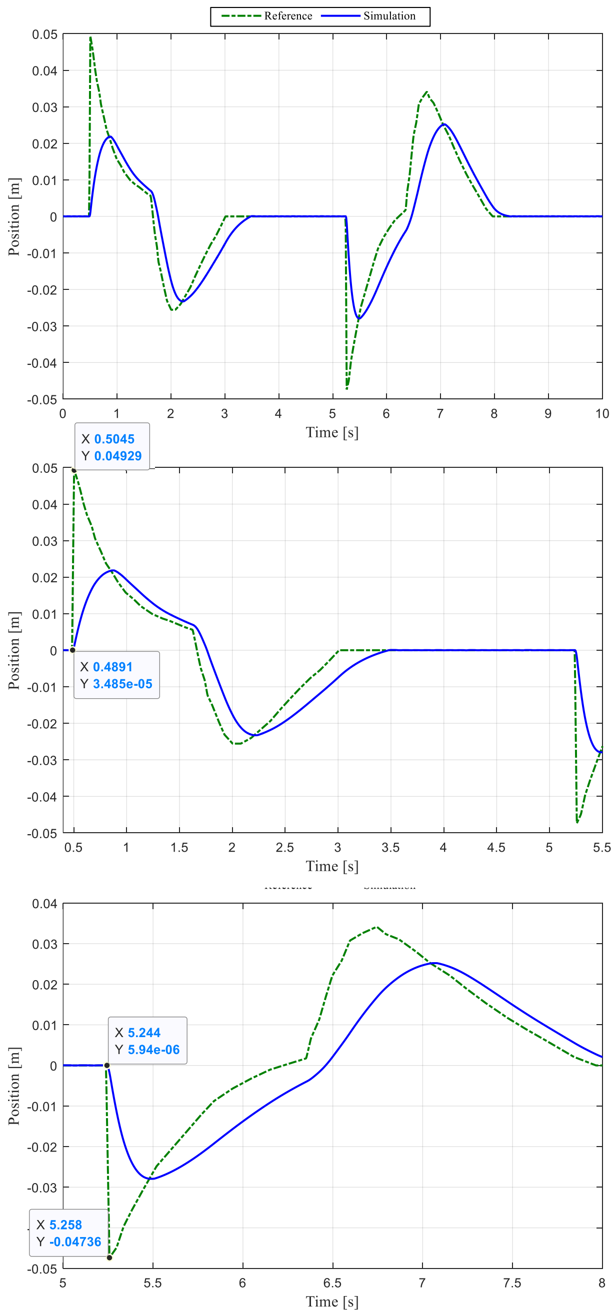

Source: By the author.

The reference input combines impulse and ramp signals, imposing rapid flow rate demands on the system. In Figure 5.14, the accumulator compensates during these moments by providing additional flow to the actuator. However, the flow rate required exceeded the system's supply capacity, causing delays in the actuator's response. Once the actuator reaches a hold position, the flow demand decreases, and the accumulator refills to prepare for the next action.

This behavior underscores the importance of optimizing hydraulic systems for specific trajectory profiles. In this case, the system was designed for longer settling times, making it unsuitable for fast, abrupt inputs. For instance, achieving a settling time t_s of 0.1 seconds would require significantly higher flow rates, approximately 105.45 L/min, while maintaining all other parameters unchanged.

Figure 5.14 – Flow rates for position control with aileron reference.

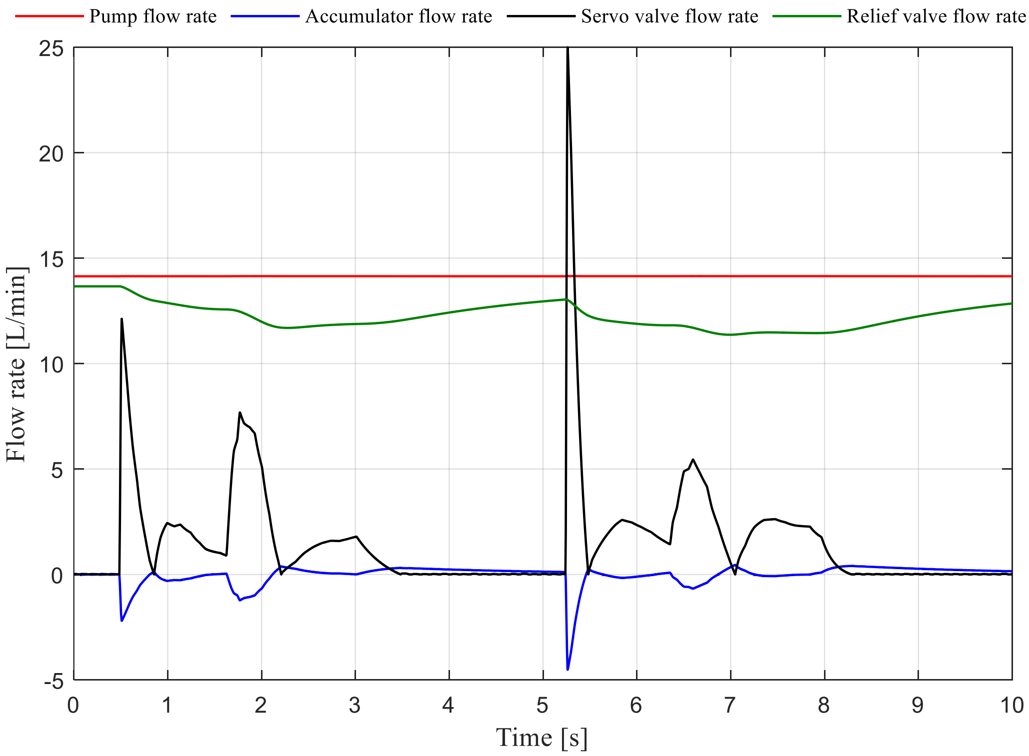

Source: By the author.

6. CONCLUSION

The primary objective of this bachelor thesis was to develop and analyze a pressurized hydraulic system for aircraft applications, with a focus on modeling and simulating the behavior of a bootstrap reservoir. The expected result was to achieve stable reservoir pressure and position control for the actuator under varying operational conditions. The simulation results confirmed that the system met these expectations, demonstrating stable pressure regulation, even during high-demand scenarios, and achieving a settling time of 0.975 seconds, which was well within the design specification of 1 second. These results validate the precision of the proposed hydraulic system design.

The study of pressurized reservoirs included a comprehensive literature review, with a primary focus on comparing the most common types, such as air-pressurized, gas-pressurized, and bootstrap reservoirs. This review analyzed their advantages, limitations, and suitability for aircraft applications.

For component sizing, the methodology proposed by Furst & De Negri (2002) was applied to determine the actuator and servo-valve dimensions necessary to meet system response requirements. The designed system achieved the desired accommodation time of 1 second, with a simulated value of 0.975 seconds, confirming that the design met the expected dynamic response. A supply pressure of 70 bar and a reservoir area ratio of 0.04 were used, resulting in a reservoir pressure of 2.8 bar, as verified in the simulation.

Additionally, a relationship between the actuator areas from the bootstrap reservoir was established. This relationship allows to size the reservoir pressure to maintain sufficient suction pressure for pump operation, ensuring system stability under varying operational conditions. By utilizing the supply pressure (p_S) and the bootstrap reservoir area ratio (A_{ratio}), the resulting reservoir pressure (p_T) can be found. Simulation demonstrated that the reservoir pressure is determined by force transmission in the bootstrap reservoir and is independent of both the available reservoir volume or its position.

Finally, the results obtained in this thesis for the bootstrap reservoir provide a basis for integration into more complex aircraft hydraulic systems, such as those proposed by Belan (2018).

6.1. FUTURE RESEARCHES

For future researches to continue the development of bootstrap reservoir, the following studies are suggested:

- Modeling with Variable Displacement Pumps: Investigate system behavior using a mathematical model of a variable displacement pump.
- Accumulator Analysis: Conduct a detailed study of the accumulator performance and integration within the system, such as pump failure and more flow rate being requested by the control surface actuator.
- Reliability Assessment: Analyze the reliability of the bootstrap reservoir under failure conditions, such as filter clogging and component wear.
- Vibration Study: Examine the vibrations in the pressurized reservoir caused by the actuator rod constant movement, requested by the control surface actuator.
- Integration with Digital Actuator: Implement findings from Belan (2018) to include reservoir dynamics in a digital hydraulic actuator model.

7. REFERENCES

AALTONEN, J. Interaction of Bootstrap Reservoir and Hydraulic Pump in Aircraft Hydraulic Systems. Tampere University of Technology, 2016.

WAHEED, A. Failure forecast of Boeing 737 bleed air system using artificial neural networks. 2011.

AMIRANTE, R., ANDREA CATALANO, L., TAMBURRANO, P. The importance of a full 3D fluid dynamic analysis to evaluate the flow forces in a hydraulic directional proportional valve. Engineering Computations, v. 31, n. 5, p. 898–922, 1 jul. 2014.

BOSCH REXROTH. Pressure relief valve, direct-operated DBD – Data sheet RE25402. 01-01-2024. Available at: https://www.boschrexroth.com/media/d9755dd3-57ed-45d9-8e9b-f8f11479fa21. Accessed on: 19 Aug. 2024a.

BOSCH REXROTH. Hydraulic Cylinder R900999T33. Available at: https://store.boschrexroth.com/Hydraulics/Cylinders/Tie-rod-cylinders/HYDRAULIC-CYLINDER_R900999T33?cclcl=en_XK. Accessed on: 05 Sept. 2024b.

BOSCH REXROTH. Axial Piston Variable Pump A10VO Series 52 and 53. RE 92703/2024-06-17. Available at: https://www.boschrexroth.com/media/c18ac983-b782-49f8-a004-75537dffb043. Accessed on: 05 Sept. 2024c.

BORUTZKY, W., BARNARD, B., THOMA, J. An orifice flow model for laminar and turbulent conditions. Simulation Modelling Practice and Theory, v. 10, n. 3-4, p. 141–152, nov. 2002.

BUDIYONO, A., JENIE, S. D. Automatic Flight Control System: Classical Approach and Modern Control Perspective. Bandung Institute of Technology, 2006.

CANUDAS DE WIT, C.; OLSSON, H.; ASTROM, K. J.; LISCHINSKY, P. A new model for control of systems with friction. IEEE Transactions on Automatic Control, v. 40, n. 3, p. 419-425, Mar. 1995. DOI: 10.1109/9.376053.

CHURN, P. M., MAXWELL, C.J., SCHOFIELD, N., HOWE, D., POWELL, D.J. Electro-hydraulic actuation of primary flight control surfaces. 1 jan. 1998.

COLLINSON, G. Fly-By-Wire. Springer eBooks, p. 115–164, 1 jan. 2023.

CRUZ, D. P. M. Análise de sistema hidráulico digital para aviões com foco em eficiência energética. 2018. 140 p. Dissertação de Mestrado. Universidade Federal de Santa Catarina.

DA COSTA, A., VILLENEUVE, M. Recent developments in high pressure maintenance free accumulators for 5000 PSI aircraft hydraulics. International Conference on Recent Advances in Aerospace Actuation Systems and Components, 2004. p. 147–152.

DE NEGRI, V. J. Sistemas Hidráulicos e Pneumáticos para Automação e Controle: Parte III - Sistemas Hidráulicos para Controle. Universidade Federal de Santa Catarina. Florianópolis, p. 80. 2001.

DESTRO, M. Análise de condições operacionais críticas em posicionadores eletro-hidráulicos. 2014. 138 p. Dissertação (Mestrado em Engenharia Mecânica). Universidade Federal de Santa Catarina, Florianópolis.

DICK, W.K. The New York Air Brake Company. Gas-charged accumulator-reservior unit. United States patent US 3047023, 31 jul. 1962.

ELLMAN, A., VIRVALO, T. Formation of pressure gain in hydraulic servovalves and its significance in system behavior, Proceedings of the ASME Fluid Power Systems and Technology, Vol. 3, 1996, pp. 77–81.

FAVRE, C. Fly-by-Wire for commercial aircraft: the Airbus experience. International Journal of Control, v. 59, n. 1, p. 139–157, jan. 1994.

FIELDING, C. The design of Fly-by-Wire flight control systems. The Aeronautical Journal, v. 105, n. 1051, p. 543–549, set. 2001.

FORD, T. Actuation systems development. Aircraft Engineering and Aerospace Technology, v. 70, n. 4, p. 265–270, ago. 1998.

FURST, F. L. Sistematização do projeto preliminar de circuitos hidráulicos de controle de posição. 2001. 149 p. Dissertação (Mestrado em Engenharia Mecânica). Universidade Federal de Santa Catarina, Florianópolis.

FURST, F.L., DE NEGRI, V. J. Projeto de sistemas hidráulicos de controle de posição. Apostila. Florianópolis: 125 p. 2002.

GARG, G. C. A., LINDA, R. I., CHOWDHURY, T., Evolution of Aircraft Flight Control System and Fly-by-Light Flight Control System. International Journal of Emerging Technology and Advanced Engineering. Vol 3 Issue 12, December, 2013.

GOMES, S. C. P.; ROSA, V. S. D. A New Approach to Compensate Friction in Robotic Actuators. Proceedings of the IEEE International Conference on Robotics & Automation. Taipei: IEEE. 2003. p. 622 – 627.

GONZALEZ, F. E. Estudo das forças atuantes em mecanismos de regulação de ângulo de passo e desenvolvimento de um sistema emulador de cargas. 2012. 168 p. Dissertação (Mestrado em Engenharia Mecânica) – Universidade Federal de Santa Catarina, Florianópolis, 2012.

GORDIĆ, D., BABIĆ, M., MILOVANOVIĆ, D., SAVIĆ, S. Spool valve leakage behaviour. Arch. Civ. Mech. Eng. 2011, 11, 859–866.

GOODEN, R.A. United Aircraft Products Inc. Bootstrap reservior. United States patent US 4538972, 3 set. 1985.

MERRIT, H.E. Hydraulic control systems. New York: John Wiley & Sons – 1967.

HUNT, T., VAUGHAN, N. The hydraulic handbook. 9th edition. Oxford, UK: Elsevier. 1996.

HYDAC Technology GmbH. Metal bellows accumulators. Sulzbach/Saar: HYDAC Technology GmbH, 2024. Available at: https://www.hydac.com/shop/pt-br/acumuladores-hidraulicos/acumuladores-de-fole-metalico. Accessed: 18 Sept. 2024.

KARLSSON, H. Styrsystemservon För Jas 39 Gripen. Utdrag ur IVASymposiumet Teknikspridning Fran Industrigruppen JAS Forskning vid Svenska Högskolor (in Swedish), Linköping, Sweden, 1985.

KOLLEK, W., KUDZMA, Z., STOSIAK, M. Possibilities of diagnosing cavitation in hydraulic systems. Archives of Civil and Mechanical Engineering, v. 7, n. 1, p. 61–73, 1 jan. 2007.

KRUS, P., BRAUN, R., NORDIN, P., ERIKSSON, B. Aircraft System Simulation for Preliminary Design. 28th International Congress of the Aeronautical Sciences, Brisbane, Australia, 2012.

LEDEZMA, J. A. P. Controle robusto de força em atuadores hidráulicos aplicando a Teoria de Realimentação Quantitativa. 2012. Dissertação (Programa de Pós Graduação em Engenharia Mecânica), 205 p. Universidade Federal de Santa Catarina.

LEI, J. Flow model and dynamic characteristics of a direct spring-loaded poppet relief valve. Proceedings of the Institution of Mechanical Engineers. Part C, Journal of mechanical engineering science, v. 232, n. 9, p. 1657–1664, 2 may. 2017.

LOCATELI, C. C. Modelagem e desenvolvimento de um sistema de controle de posição pneumático com acionamento por válvulas on/off. 2011. Dissertação (Programa de Pós Graduação em Engenharia Mecânica), 114 p. Universidade Federal de Santa Catarina.

LINSINGEN, Irlan von. Fundamentos de sistemas hidráulicos. Quarta edição revisada. Florianópolis: Editora da UFSC, 2013. 400 p.

MAKKAR, C.; DIXON, W. E.; SAWYER, W. G.; HU, G. A new continuously differentiable friction model for control systems design. In: IEEE/ASME INTERNATIONAL CONFERENCE ON ADVANCED INTELLIGENT MECHATRONICS, 2005, Monterey, CA, USA. Proceedings [...]. Monterey, CA: IEEE, 2005. p. 600-605. DOI: 10.1109/AIM.2005.1511048.

MARÉ, J. C., Aerospace Actuators 1: Needs, Reliability and Hydraulic Power Solutions. John Wiley & Sons, Inc. 2016.

MARÉ, J. C., Aerospace Actuators 2: Signal-by-Wire and Power-by-Wire. John Wiley & Sons, Inc. 2017.

MICHAEL, V.G. Martin-Marietta Corporation. Combination reservior-accumulator arrangement for hydraulic system. United States patent US 3015345, 2 jan. 1962.

MOIR, I., SEABRIDGE, A. Aircraft Systems: Mechanical, electrical, and avionics subsystems integration. 3rd Ed. John Wiley & Sons, Ltd. ISBN 978-0-470-05996-8. 2008.

MURARO, I. Estudo das Características Comportamentais de Válvulas Proporcionais e seus Efeitos nos Posicionadores Eletro-Hidráulicos. 2009. Dissertação (Programa de Pós Graduação em Engenharia Mecânica), 176 p. Universidade Federal de Santa Catarina.

NOSTRANI, M. P. Development of a Digital Electro Hydrostatic Actuator for Application in Aircraft Flight Control Surfaces. 192 p. Tese em Engenharia Mecânica. Universidade Federal de Santa Catarina, Florianópolis. 2021.

OGATA, K. Modern Control Engineering. 5th ed. Upper Saddle River: Prentice Hall, 2010.

ORLEBAR, C. Concorde: The story of the supersonic airlines. Oxford: Osprey Publishing, 2010.

OUYANG, X.P. Hyundai Aircraft Hydraulic Technology; Zhejiang University Press: Hangzhou, China, 2016.

OUYANG, X.P., WANG, T.Z., XU, F. Research Status of the High Speed Aircraft Piston Pump. Chinese Hydraulics & Pneumatics, n. 2, p. 1, 15 feb. 2018.

PINTO, L. O. G., BELAN. H. C, LOCATELLI, C. C., KRUS, P., DE NEGRI, V. J., LANTTO, B. New Perspectives on Digital Hydraulics for Aerospace Application. Aerospace Technology Congress. Solna. October 11-12, Stockholm. 2016.

PLUMMER, A. 2016. Electrohydraulic servovalves – past, present, and future. 10th international fluid power conference (IFK2016), 405–424.

SILVA NETO, N. W. da. Metodologia de dimensionamento de acumuladores hidráulicos para controle de força. 2021. 82 p. Dissertação (Programa de Pós Graduação em Engenharia Mecânica) – Universidade Federal de Santa Catarina.

SZPAK, R. Análise Teórico-Experimental do comportamento das pressões em posicionadores hidráulicos. 2008. Dissertação (Mestrado em Engenharia Mecânica). Universidade Federal de Santa Catarina, Florianópolis.

TAMBURRANO, P. et al. A review of electro-hydraulic servovalve research and development. International Journal of Fluid Power, p. 1–23, 30 out. 2018.

TAMBURRANO, P. Internal leakage in the main stage of servovalves: An analytical and CFD analysis. AIP conference proceedings, 1 jan. 2019.

TRAVERSE, P., LACAZE, I., SOUYRIS, J. Airbus Fly-By-Wire: A Total Approach To Dependability. IFIP International Federation for Information Processing, 2004.

VACCA, A., FRANZONI, G. Hydraulic Fluid Power: Fundamentals, Applications, and Circuit Design. John Wiley & Sons, 2021. 704 p.

VALDIERO, A. C. Controle de robôs hidráulicos com compensação de atrito. Tese de doutorado - Universidade Federal de Santa Catarina, Centro Tecnológico, Programa de Pós Graduação em Engenharia mecânica, Florianópolis, 2005.

XIAO, W.J., HU, H., WIE, L.J Hydraulic Tank of a Fighter: Fault Analysis and Improvement. Chinese Hydraulics & Pneumatics, 2013.

XU, X., ZHANG, P., ZHOU, Q. Analysis and Improvement on Asymmetrical Wear in Aircraft Bootstrap Reservoir. Lecture notes in electrical engineering, p. 728–734, 2 nov. 2021.

YANG, C., DU, L.L, QING, H, YANG, J. The design of pressurized tank test bench for a certain airplane hydraulic system[J]. Chinese Hydraulics & Pneumatics, 2012, 0(2): 103-105.

ZHANG, C., ZHU, C., MENG, B. Challenges and Solutions for High-Speed Aviation Piston Pumps: A Review. Aerospace, v. 8, n. 12, p. 392–392, 10 dez. 2021.